The Distribution and Characterization of Suspended Particles in Pohjanpitäjänlahti Estuary

Jonas Jan Erik Hjort, 37842
Master´s Thesis in Environmental Geochemistry
Supervisors: Peter Österholm and Joonas Virtasalo
The Faculty of Engineering and Natural Science, Geology and Mineralogy
Åbo Akademi University
November 2020

Abstract

Suspensions of eroded minerals and organic matter, as well as particulate and dissolved elements such as Fe and Mn, are transported from land to sea and ultimately deposited in sediments. These materials have a strong impact on biogeochemical processes, including nutrient cycling in coastal sea areas and in sediments. Hence, it is important to understand the factors controlling their transport and sedimentation. For iron (Fe) and manganese (Mn), redox driven precipitation and re-mobilization of oxides is an important process in coastal environments. They may occur in a soluble form when discharged in to the estuary, and precipitate in to particles in the brackish high-pH surface waters. If sedimented, Fe and Mn are dissolved under anoxic conditions in sediments or near-bottom water. The dissolved Fe and Mn in the porewater may then move upwards in the sediment and further to the water column until they reach oxidizing conditions, and precipitate as oxides. These oxides may co-precipitate phosphates (reducing eutrophication) and/or function as electron acceptors in organic matter respiration in the absence of oxygen.

As a part of a larger project, in which suspended particles and estuarine biogeochemistry are studied, the aims of this study are (1) to quantify and characterize suspended inorganic particles in an estuarine environment, (2) to facilitate the use of a LISST-100X suspended particle size analyzer in *in situ* marine studies, and (3) to understand the redox driven Mn cycling in the estuarine environment. The study site is the *Pohjanpitäjänlahti* estuarine transect in southern Finland (Gulf of Finland). A total of 12 study sites (A-C, C2, D-K) were visited along the estuarine transect during the FINMARI cruise in October 2018 onboard the r/v Geomari of the Geological Survey of Finland. Continuous particle size distribution profiles of the water column at the study sites were obtained by the LISST-100X instrument, which measures *in-situ* sizes and volume concentrations of particles suspended in the water column by laser diffraction method. Continuous salinity and temperature profiles were collected by an EXO2 multiparameter sonde. Water samples from selected depths were collected at each station and filtered with a precombusted 0.7 µm fiberglass filter. From the retentates collected on the filters, particle sizes, particle compositions and element associations were characterized with scanning electron microscope (SEM) and energy-dispersive X-ray spectroscopy (EDS). The suspended particles were a mixture of mineral grains, diatoms and organic material, all with sizes below 10 µm dominating. Larger particles were typically aggregates of clay minerals and organic matter. The bottom waters were generally dominated by coarser particles (103 –

200 μm) while finer particles (1,0 – 10,2μm) were mostly found in the surface waters. Due to seasonal variations and topographical irregularities a part of the estuary experiences hypoxic/anoxic conditions in the bottom water. In these waters Mn concentrations exceed the average amounts along the rest of the estuarine transect. Manganese morphotypes of varying sizes (mostly 3 – 7 μm) and with distinctive large cauliflower and small star-shaped morphologies were also found in sections of the estuary.

Table of contents

1. Introduction

1.1 Introduction to Suspended Particles in water

Suspended particles (SP) are invariably present in natural water bodies. A particle may consist of a various selection of materials, from clay and precipitates to biogenic particles such as phytoplankton cells, diatoms, and algae. Particles in streams and rivers are usually derived from the bedrock and soil in the catchment area. Streams also carry significant amounts of humified organic matter, dissolved or colloidal humus, in to the estuary. Due to random collisions between SP they are attaching to each other creating aggregates (Maggi, 2005). Larger and/or heavier aggregates containing silicates and metallic precipitates, later settle on the seafloor where they are accumulated as a sediment. After accumulation, resuspension processes may convey particles back into suspension (Fig. 1). Another particle forming process is flocculation, which causes small particles to coagulate due to chemical attraction between particles, often because of increasing salinity levels in the surrounding water (Van Leussen, 1988). Flocculation processes are especially common in estuarine environments due to sudden chemical changes when freshwater mixes with seawater (Asmala et al, 2014).

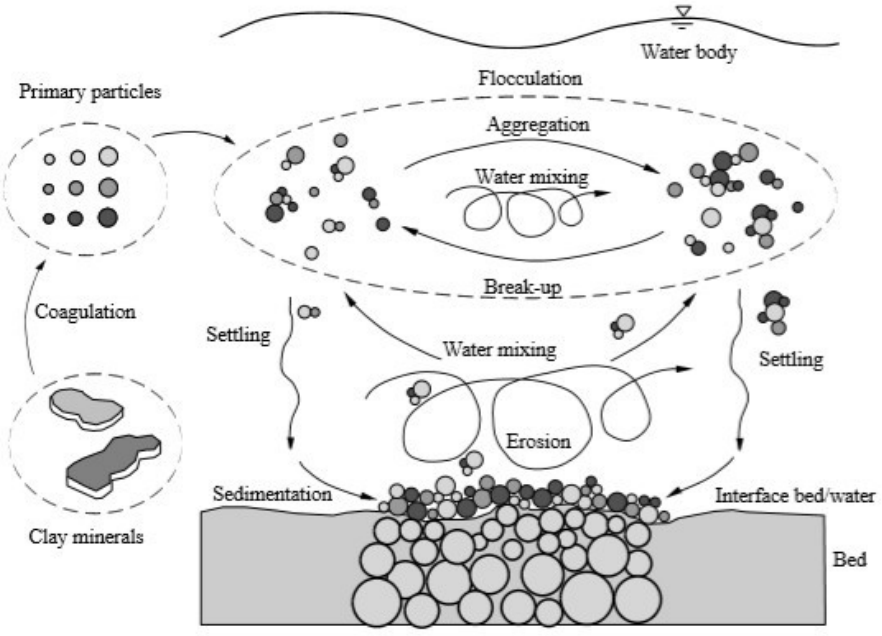

Figure 1. The build-up and break-up cycle of particle aggregation with sedimentation and resuspension processes (Maggi, 2005).

1.2 Manganese in marine environments

Manganese (Mn) is one of the most common metals in the earth's crust and exists as a major element in many mineral configurations. Mn is easily depleted from igneous and metamorphic rocks and is highly mobile as Mn-oxyhydroxide in aqueous systems (Hein et al. 2016). Dissolved and/or particulate Mn in rocks and bedrock is weathered and transported to rivers, lakes, and estuaries with the help of ground, and surface water (Post, 1999).

Mn is easily oxidized, making it sensitive to redox conditions. Redox transitions between Mn (II), Mn (III) and Mn (IV) oxy-hydroxides, are common and important processes in natural waters. These transitions control the partitioning of Mn between dissolved and particulate (solid) phases in waters and sediments, and thereby regulate the scavenging of Mn from the water columns of lakes, rivers, and oceans as well as its transfer from sediments back into overlying waters (Sunda & Huntsaman, 1990). Dissolved Mn and iron (Fe) may also precipitate together or separately as phosphate oxides removing plant-fertilizing phosphate dissolved in the water, hence counteract eutrophication (Gaosheng et al. 2009).

1.3 Objectives

This thesis has essentially three main objectives. The first objective is to quantify and characterize suspended particles (SP) along the Pohjanpitäjänlahti estuarine transect. As a second objective, the advantageous uses of the LISST-100X particle size analyzer in *in-situ* marine studies will be discussed. After the quantification and characterization of the SP is presented, the focus will be to understand the redox-driven manganese cycling in the estuarine environment.

2. Material and Methods

2.1 Study area

Pohjanpitäjänlahti (Swedish: *Pojoviken*) is a northeast-southwest trending estuary located in the municipalities of Raasepori and Hanko in southern Finland (Fig. 2). The estuary measures between 0,2 - 3 km in width and has a length of approximately 30 km making it noticeably narrow in many places. To the north, freshwater is discharged into the estuary from the Mustionjoki river, which is the main freshwater source (Tiihonen, 2016). An ice-marginal ridge formation (*Salpausselkä I*), deposited during the retreat of the Fennoscandian ice-sheet, is crossing the estuarine transect in the middle, in a south-western direction, forming a shallower section near the town of Tammisaari (Jilbert et al., 2018). The studied estuarine transect can therefore be divided into three sections, the Pohjanpitäjänlahti estuary (stations A to E) and archipelago (stations H to K), both exceeding 30 m in the deepest parts. Between the estuary and archipelago, the shallower sill section (stations F and G) is connecting the two, making it a mixing zone between freshwater from the north and seawater from the Gulf of Finland in the south.

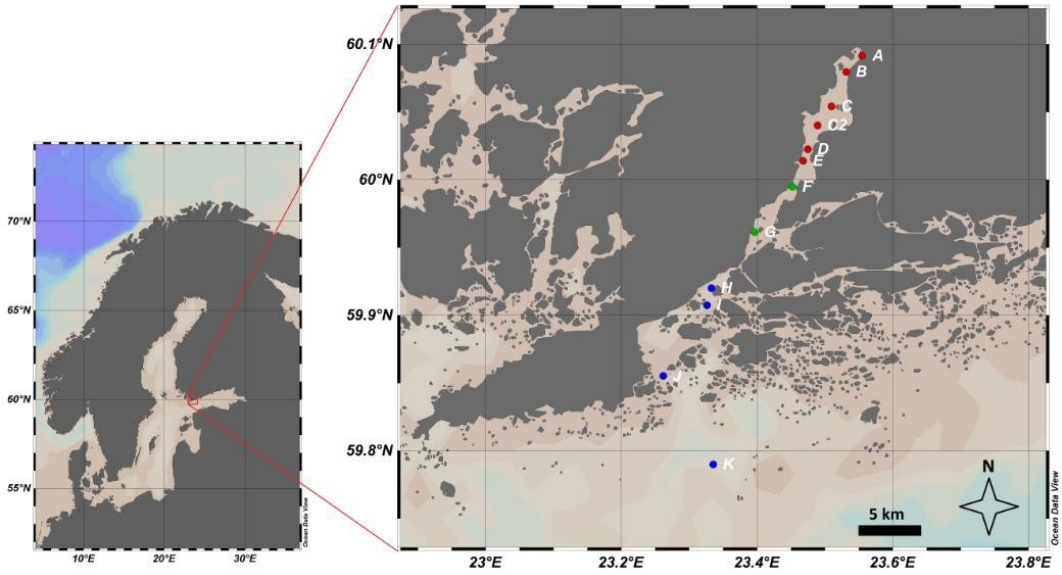

Figure 2. Map of the study site in Pohjanpitäjänlahti estuary, with stations A – E (red) in the estuary, F – G (green) in the sill section, and H – K (blue) in the archipelago.

2.2 Sampling

The samples that have been processed in this thesis are gathered from the 12 marine sampling stations along the estuarine transect (A – C, C2, D – K) (Fig. 2). The sampling trip took place in October 2018 onboard the research vessel Geomari, departing from the Tvärminne research station in Hanko. Because of seasonal cycling, autumns in this region are characterized by low riverine discharge. The sparse flux of freshwater from the rivers may cause the seawater to enter the inner basin resulting in water mixing. This variable may be good to consider if a comparison with previous studies are made.

2.3 Submersible instruments

Suspended particle size distribution and concentration as well as physical and chemical variables were measured by using submersible instruments along the estuarine transect. The primarily measurements were done using an YSI™ EXO2 multiparameter sonde and a Sequoia LISST-100X type B. Additional data were also collected and to some extent used by a Sea & Sun Technology CTD 90 M Series II sonde. The instruments were all attached to a steel frame, which was secured and lowered by a wire crane aboard the vessel (Fig. 3). By lowering all instruments at the same time, the collected data could be supplemented with each other.

2.3.1 YSI™ EXO2 and Sea & Sun Technology CTD 90 M Series II

An YSI™ EXO2 multiparameter sonde (EXO2) measures water characteristics in the water column. It is widely used in oceanographic, estuarine, and surface water applications and it is rated to a depth of 250 m. Some of the parameters that the EXO2 measures is water temperature, conductivity (salinity), pressure (depth), dissolved oxygen, pH, and turbidity (YSI, 2020). In addition to the EXO2 a Sea & Sun Technology CTD 90 M series II (CTD) (Fig. 3) were used to support the EXO2 measurements. Sea & Sun CTD measures the same parameters as EXO2 except pH-values.

2.3.2 Sequoia, LISST-100X

The Sequoia LISST-100X laser in-situ scattering and transmissometry multi-parameter system was used to gather data over suspended particle size distribution

and concentration. The LISST device is a submersible tool that is designed to do *in-situ* measurements of particle size distributions and particle volume concentrations in marine environments. The LISST gathers information on many different physical and chemical variables in the water (Sequoia, 2020).

The most important are:

- Particle volume concentrations in µl/l, with different sizes, ranged from 1,09 – 184,11 µm (specific to type B with the random shape particle model), divided into 32 size bins.
- Water pressure (depth in meters)
- Water temperature (in Celsius)

The raw data measured by the LISST was later merged with EXO2 and CTD data into an excel sheet. The data was cleaned by calculating the median value from each meter's depth, to make it easier for further interpretations. Medians were used instead of means to reduce the effects of potential outliers.

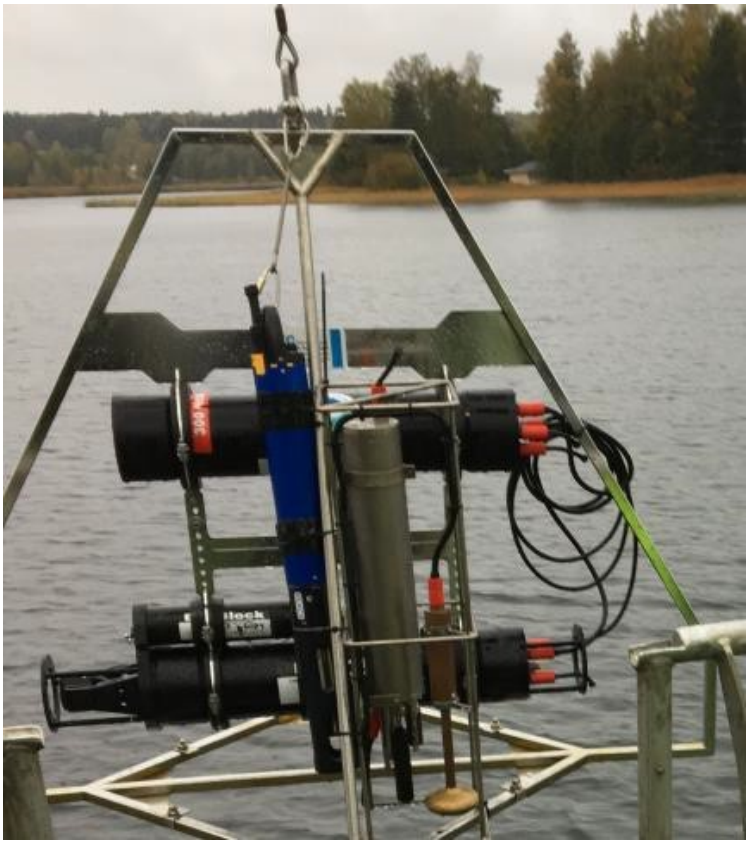

Figure 3. The LISST-100X instrument (black horizontal tubes), the EXO2 (blue sonde) and the CTD (metallic sonde) attached to a steel frame aboard R/V Geomari.

2.4 Water column sampling

The Limnos sampling is a technique used to collect water samples from certain depths of the water column. The Limnos sampler (Fig. 4) is a plastic tube designed to be submerged into the water while attached to a line. The tube holds up to 2,5 l and is suitable for small water sampling jobs. When the sampler is located at a preferred depth a weight is sent down the line activating flaps on the tube, which closes and encases the water inside. After retrieving the Limnos tube, the water inside is carefully transferred to labeled bottles for further analyzes. For this study, a total of 79 water samples were taken at different depths along the estuary (Table. 1)

Figure 4. The Limnos water sampler used in this study (here open and ready for use). The sampler is attached to a line with depth markings. The sampling tube is then submerged to a preferred sampling depth. Two flaps at the top and bottom of the tube are then closed by sending down a metallic weight down the line. When the weight reaches the tube, a mechanism closes the flaps enclosing the water inside the tube.

2.5 Retentates

To analyze SP in the Limnos water samples, a water filtering process was carried out. The water was filtered through 0,7 µm *Whatman* filters that captured single particles and aggregates suspended in the water. From every water sample around

300 ml of water was filtrated trough labeled filters. The filters were then freeze-dried to retain the mineral particles, as well as the organic material. Selected dried filters (listed in Table 1) were later inserted in a scanning electrode microscope (SEM), in which electron dispersive x-ray spectroscopy (EDS) analyzes were done. The purpose of these analyzes was to determine the size, form, and composition of the particles in the retentate.

In a parallel study with aliquots of the same water samples (Newton, 2019), a different filtration process was done by filtrating some of the same samples through three filters, 10µm, 3µm and 1µm. These filters were then digested and sent to the commercial laboratory Labtium Ltd, for ICP-MS analyzes, together with the remaining filtrate. The water samples that were analyzed are listed in Table 1.

Table 1. Table representing every water sample taken from different depths at every station. Samples that have been analyzed; with SEM labeled with (S), ICP-MS analyzes (M), and samples not analyzed but taken (x)

Stations	A	B	C	C2	D	E	F	G	H	I	J	K
0m	SM	SM	M	M	M	SM	SM	SM	M	SM	M	M
2m	SM	M	M	M	SM	SM	SM	M	M	M	SM	M
4m	M	SM	x	S	M	x	x	SM	S	x	S	x
6m	SM	SM	SM	M	M	S	M	SM	x			
8m		S	S	S	SM	S	x					
10m		x	SM	SM	SM	S			x	x	x	
15m			x	x	M	M			SM	M		S
20m			x	x	M	S				S	x	
25m				x	M							
30m					M						x	x
35m					SM							
45m												S

2.5.1 Filter retentate preparation for SEM analyzes

To be able to insert the filters into the SEM, the filters needed to be prepared in a certain way to obtain usable results. The SEM assemblage often uses thin sections for routine analyzes. In this case a selection of filters (36 in total) were assembled onto thin sections using two-sided graphite tape. The thin sections consisted of three cut-to-fit filters resulting in a total of 12 thin sections (Fig. 6a). Before SEM insertion the thin sections were coal-coated to obtain a more conductive and protecting surface (Goldstein et al. 1992). Six thin sections at a time were placed on a plate (Fig. 6b) and inserted into the SEM.

2.6 EDS method

Electron dispersive x-ray spectroscopy (EDS), is an analytical method used to determine elemental compositions or chemical characterizations of a sample. The method is based on measuring electromagnetic emissions. X-ray beams are shot at a certain area on the sample ejecting electrons from inner atom shells of elements. When the inner electrons are ejected, electrons from the outer shells "compensate" and moves to the inner shell, releasing energy as an x-ray. Due to unique atomic structures, elements have different x-ray emissions, which can be seen as peaks in a spectrum. The more of an element in a sample, the more x-ray emissions, resulting in a higher peak and thus a higher amount of that element (Goldstein et al., 2018).

The EDS-analyzes were manually done by selecting two analyze areas per filter and doing around 10 analyzes per area. The size of the areas was 115 x 115 µm (Fig. 7). To increase the chances of detecting Mn particles, denser particles found on the filters were favorably chosen.

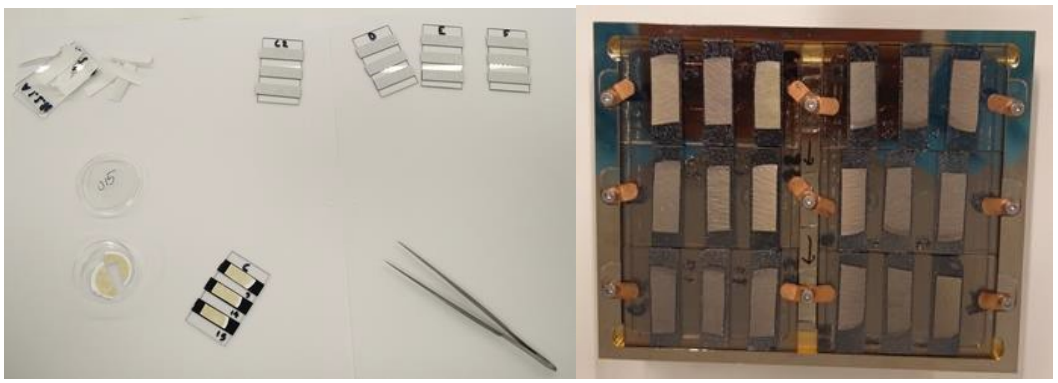

Figure 6a (left) and 6b (right). To the left, filters after the filtration process. The filters are cut and then taped by graphite tape to thin sections, three by three. In the right picture six thin sections placed on a plate ready to be inserted into the SEM.

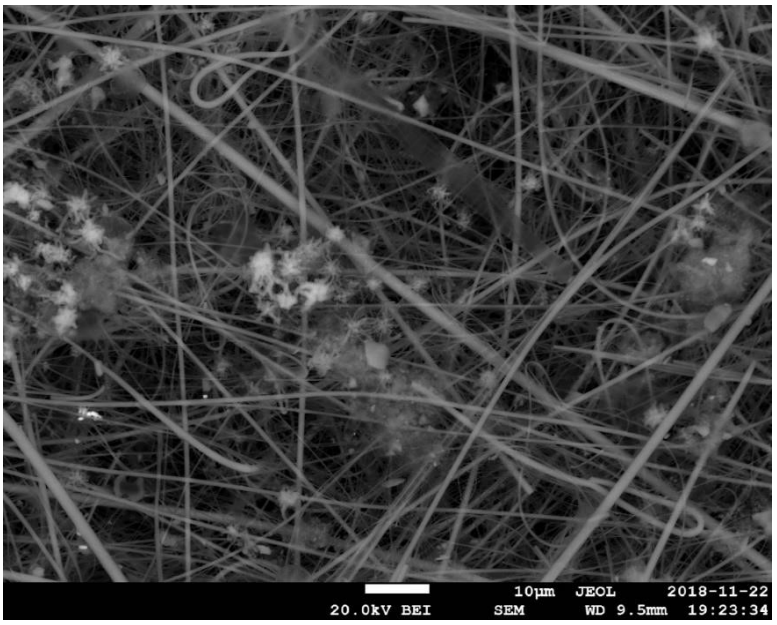

Figure 7. A SEM-picture of a filter at micro-scale, taken from station D35. The picture shows "star-shaped" Mn-rich particles and other less dense silica minerals. The long threads are glass-fibers which the filter is made of.

2.7 Visual assessment

A visual assessment of particle concentration ratios was done on SEM-pictures (Appendix B) (with a zoom of x300) to compare it with the LISST results. The reason behind the assessment is to evaluate the accuracy of the LISST instrument regarding particle size distribution measurements in the water column. The assessment was done by manually rating the number of particles in the fractions; fine (< 9,35 µm), intermediate (9,35 – 94,94 µm), and coarse (> 94,94 µm) particles in the SEM-pictures. The fractions in each picture were rated on a scale from 1 to 10, with 1 representing none or very few particles and 10 representing an abundance of particles. The ratings were determined by personal preference. After the manual particle rating of each fraction, the result was compared with LISST-data of particle size distribution presented in ratios (in %) between the same size fractions fine, intermediate, and coarse (Figure 13 - 15).

Eleven (11) SEM-pictures from ten (10) stations were chosen for this assessment; C2 10 (x2), D2, D8, D10, D35, E0, F0, G4, H4, and J2. Due to resolution quality, these stations were the only ones appropriate for assessment.

3. Results

3.1 General water characteristics of the estuarine transect

Water temperature along the estuarine transect varied between 4 – 12 ºC. In the estuary (stations A – E), apart from cooler surface water, temperatures were higher, 10 – 12 ºC at depths between 1 – 14 m (Fig. 8). The thermocline could clearly be identified in the inner estuary because of a rapid cooling of several degrees from 11 – 7 ºC over just a few meters at depths around 12 to 16 meters depending on the station (Fig. 8). Because of the shallower water at stations A and B, the temperature was rather uniform all the way to the bottom. In stations C – E, however, the thermocline stretched from depth of 12 m at station C to 13 m at C2, 16 m at D and 14 m in station E. Under the thermocline the water temperatures stabilized at 8 – 7 ºC (Fig. 8).

In the sill (station F and G) the temperatures were generally uniform throughout the water column, again with exceptions of lower surface temperatures. The only trend which is seen is that in station F the water temperature is slightly warmer than in station G (Fig. 8). Water temperatures in the archipelago (station H – K), however, are with some exceptions very uniform around 9 ºC.

The water salinity in the estuary seems to be divided into three different salinity sections, the surface 0 -1 m, the middle 1 – 10 m and the bottom section below 10 m (Fig. 9). In the surface section the water is close to fresh, near 0 psu. In the middle section water salinity is around 3 psu, and below the middle section the salinity quickly increases to around 5 psu in the bottom section. In the sill where seawater from the archipelago meets the river water from the inner estuary, a major shift in salinity can be observed (Fig. 9). In station F the salinity values correspond to the inner estuary, whereas station G obtains a larger share of seawater and therefore show salinity values up to 6 psu at the bottom. The archipelago shows little changes in salinity between the stations and has steady salinity values of 6 – 7 psu throughout the water mass, with negligible exceptions of the surface waters (Fig. 9).

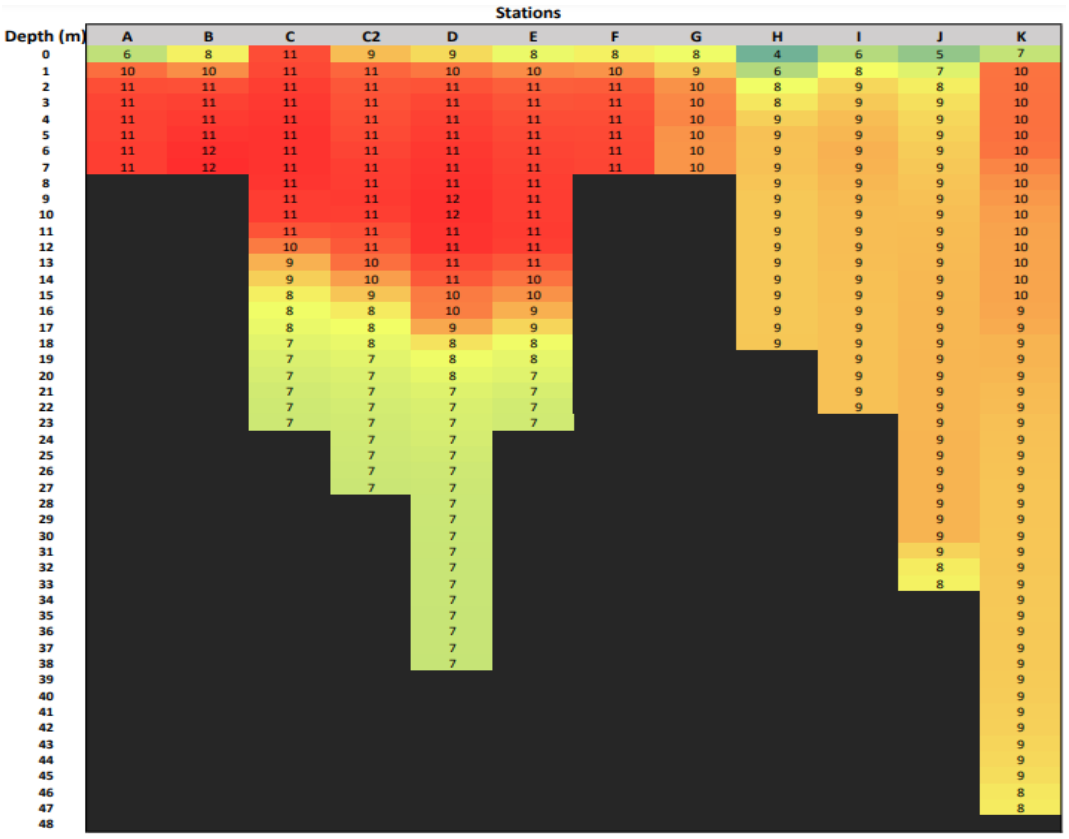

Figure 8. Temperature (ºC) along the estuarine transect.

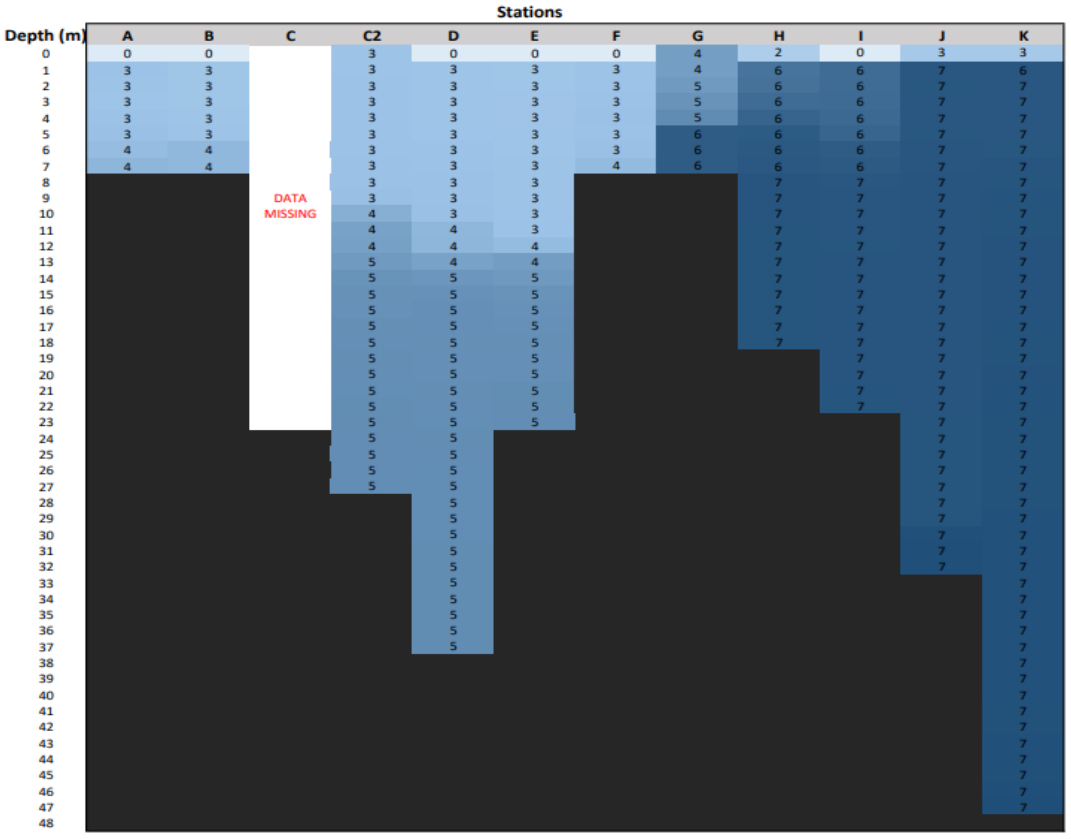

Figure 9. Salinity (psu, 0,1%) along the estuarine transect.

The thermocline and the halocline seem to be very congruent in the Pohjanpitäjänlahti estuary (Fig. 8 – 9). By combining the temperature and salinity values along the whole transect it is possible to calculate the water density at every station (Fig. 10). The water density is calculated from the previous figures (Fig. 8 – 9) according to methods gathered from Gill (1982).

The pycnocline is the interface between denser and less dense waters and can be found in every station, but is most clearly represented in the estuary and the sill section at depths between 4 – 12 m (Fig. 10), dividing the water into a surface water layer (SWL) above and a bottom water layer (BWL) below (Appendix A). In reality, the pycnocline can be several meters in depth, and should not be defined as a sharp line. An approximate pycnocline (Fig. 10) works, however, as a good tool to highlight and explain further results.

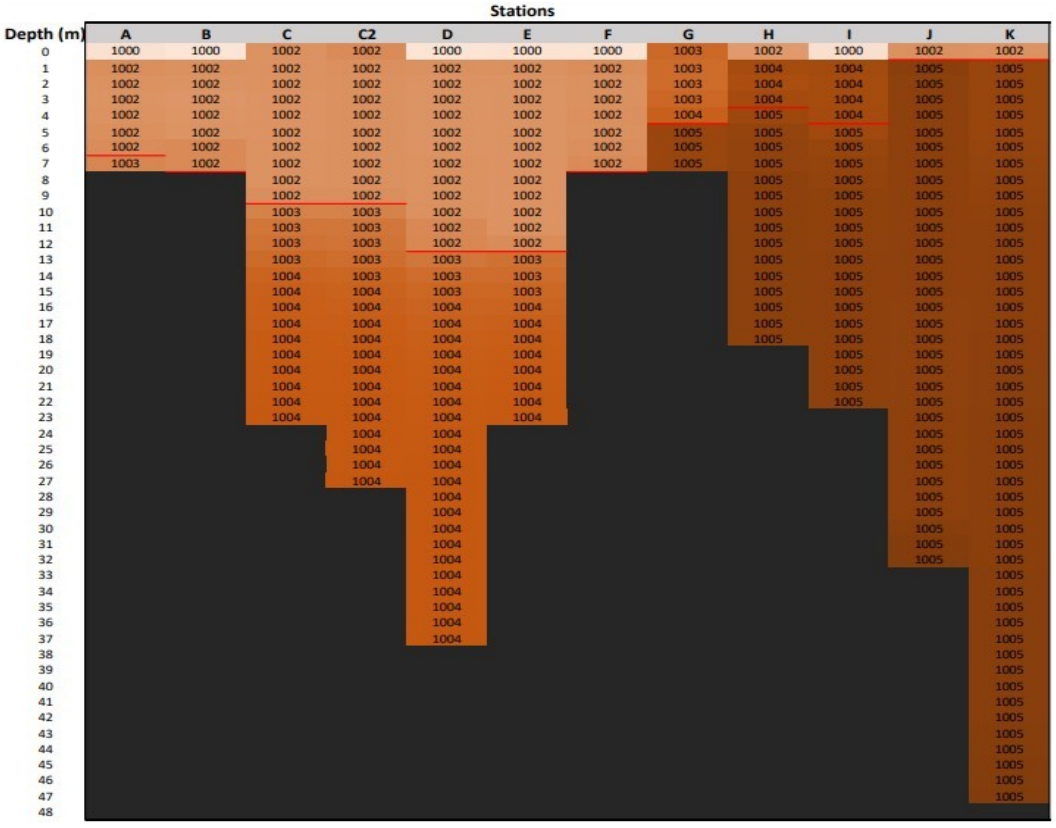

Figure 10. The water density in (g/l) of the estuary calculated from temperature and salinity. The approximate pycnocline is highlighted with red lines.

The oxygen levels were generally good throughout whole estuarine transect (around 10 mg/l), except in the BWL (below 14 – 17 m) in the estuary (Fig. 11). In this zone

the oxygen levels were hypoxic with values between 2 – 1 mg/l, and even anoxic (0 mg/l) in the deeper parts of station D (Fig. 11).

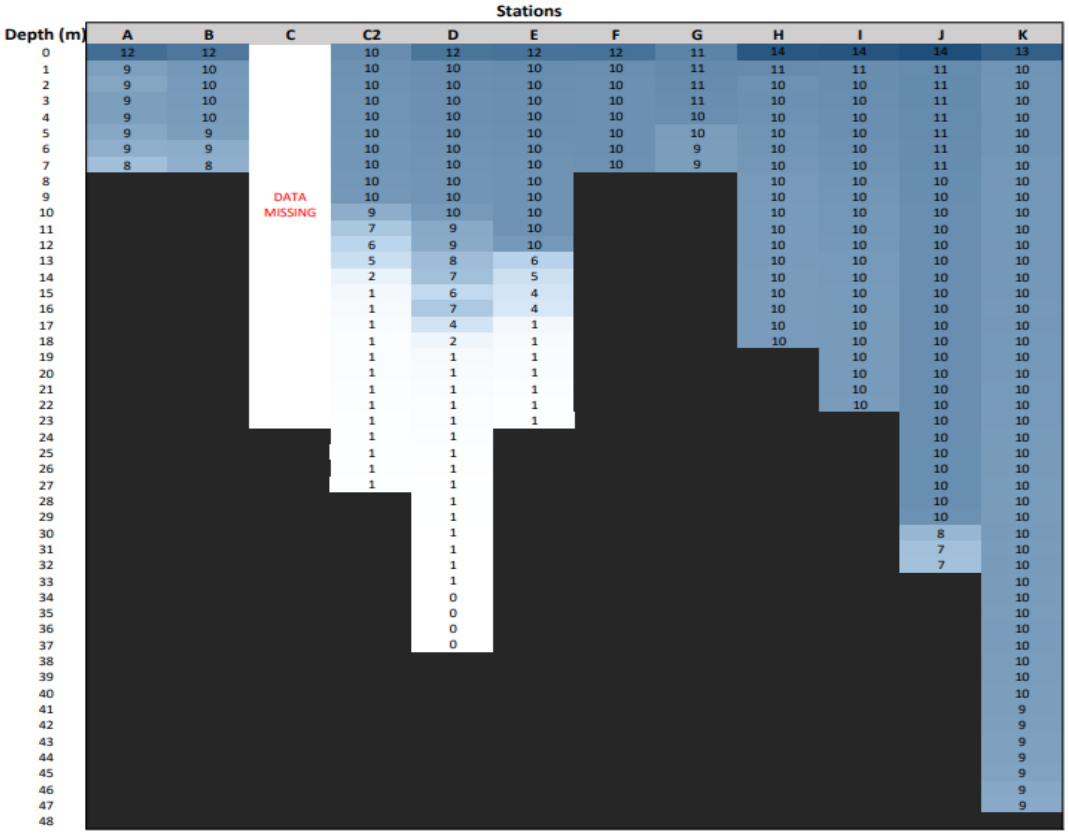

Figure 11. The amount of dissolved oxygen in the estuary (in mg/l).

3.2 Total particle volume in water columns

The distribution of particles along the estuarine transect is measured by volume concentration (ml/l). The lowest particle concentrations in the estuary were found a few meters under and a few meters above the pycnocline (< 10 ml/l) in station C and C2, and with a few exceptions, along the whole archipelago (< 7 ml/l) (Fig. 12). The highest particle concentrations were found at the river mouth and further out along the pycnocline, however, in station D the highest concentrations extended to the lower parts of the pycnocline around 16 m (Fig. 12). High particle concentrations were also found in the sill section as well as in deeper parts of station H – J. Concentration peaks (above 140 ml/l) were found in the bottom waters of station F and J.

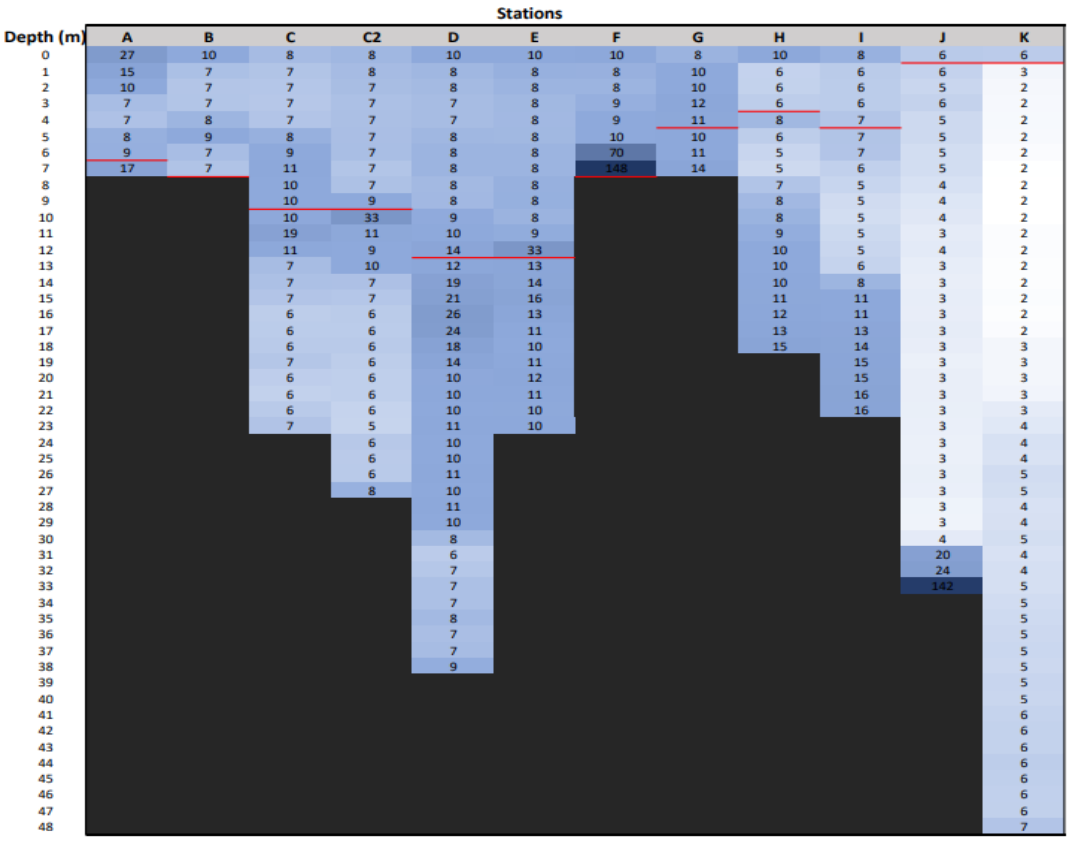

Figure 12. Total particle volume concentrations (ml/l) along the estuarine transect. Pycnocline represented by the red lines.

3.3 Particle size distribution in water columns

Figure 13 – 15 display the distribution of particle volumes in three size ranges between 1 – 200 µm, and their volume concentration (in mg/l). The LISST 100X type B divides the size ranges into 32 size classes "bins", with the smallest (bin 1) including particles between 1,00 – 1,18 µm and the largest (bin 32), including particles between 169 – 200 µm. To better explore the particle size distribution, the sizes are divided into fine particles, 1,0 – 10,2 µm (bins 1 – 14), intermediate particles, 10,2 – 103,0 µm (bins 15 – 28), and coarse particles, 103 – 200 µm (bins 29 – 32).

In the estuary fine particles are mostly concentrated to surface waters (in relation to intermediate and course particle fractions) representing more than 40% of the total particle volume (Fig. 13). In deeper waters fine particles are generally below 20% of the total particle volume. In contrast to fine particles (with exception of the river mouth) the coarse particles (103 – 200 µm) dominated the bottom water, up to 70% of the total particle volume (Fig. 15). Furthermore, there was an enrichment of

coarser particles near the pycnocline in the estuary. The intermediate particles were in relation to the fine and coarse fractions evenly distributed along the whole estuarine transect making up around 50% of the total particle volume except below the pycnocline in the estuary, where the intermediate fraction were around 30% (Fig. 14).

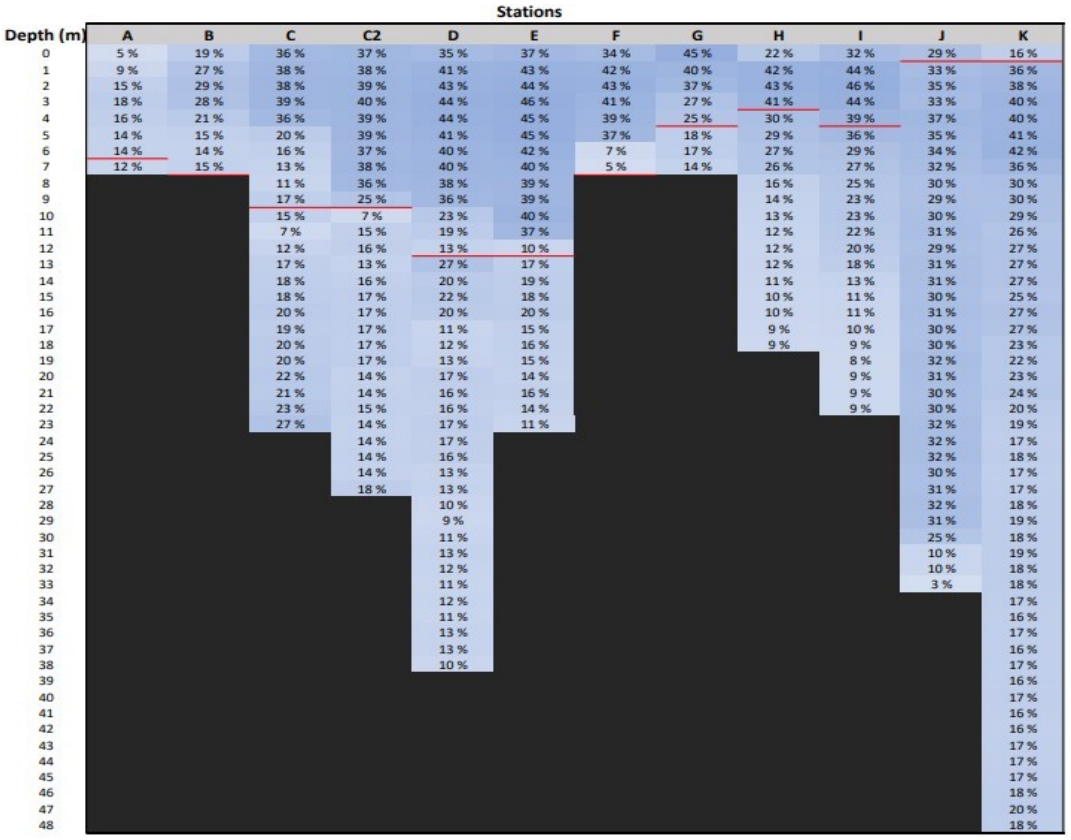

Stations

Depth (m)	A	B	C	C2	D	E	F	G	H	I	J	K
0	5 %	19 %	36 %	37 %	35 %	37 %	34 %	45 %	22 %	32 %	29 %	16 %
1	9 %	27 %	38 %	38 %	41 %	43 %	42 %	40 %	42 %	44 %	33 %	36 %
2	15 %	29 %	38 %	39 %	43 %	44 %	43 %	37 %	43 %	46 %	35 %	38 %
3	18 %	28 %	39 %	40 %	44 %	46 %	41 %	27 %	41 %	44 %	33 %	40 %
4	16 %	21 %	36 %	39 %	44 %	45 %	39 %	25 %	30 %	39 %	37 %	40 %
5	14 %	15 %	20 %	39 %	41 %	45 %	37 %	18 %	29 %	36 %	35 %	41 %
6	14 %	14 %	16 %	37 %	40 %	42 %	7 %	17 %	27 %	29 %	34 %	42 %
7	12 %	15 %	13 %	38 %	40 %	40 %	5 %	14 %	26 %	27 %	32 %	36 %
8			11 %	36 %	38 %	39 %			16 %	25 %	30 %	30 %
9			17 %	25 %	36 %	39 %			14 %	23 %	29 %	30 %
10			15 %	7 %	23 %	40 %			13 %	23 %	30 %	29 %
11			7 %	15 %	19 %	37 %			12 %	22 %	31 %	26 %
12			12 %	16 %	13 %	10 %			12 %	20 %	29 %	27 %
13			17 %	13 %	27 %	17 %			12 %	18 %	31 %	27 %
14			18 %	16 %	20 %	19 %			11 %	13 %	31 %	27 %
15			18 %	17 %	22 %	18 %			10 %	11 %	30 %	25 %
16			20 %	17 %	20 %	20 %			10 %	11 %	31 %	27 %
17			19 %	17 %	11 %	15 %			9 %	10 %	30 %	27 %
18			20 %	17 %	12 %	16 %			9 %	9 %	30 %	23 %
19			20 %	17 %	13 %	15 %				8 %	32 %	22 %
20			22 %	14 %	17 %	14 %				9 %	31 %	23 %
21			21 %	14 %	16 %	16 %				9 %	30 %	24 %
22			23 %	15 %	16 %	14 %				9 %	30 %	20 %
23			27 %	14 %	17 %	11 %					32 %	19 %
24				14 %	17 %						32 %	17 %
25				14 %	16 %						32 %	18 %
26				14 %	13 %						30 %	17 %
27				18 %	13 %						31 %	17 %
28					10 %						32 %	18 %
29					9 %						31 %	19 %
30					11 %						25 %	18 %
31					13 %						10 %	19 %
32					12 %						10 %	18 %
33					11 %						3 %	18 %
34					12 %							17 %
35					11 %							16 %
36					13 %							17 %
37					13 %							16 %
38					10 %							17 %
39												16 %
40												17 %
41												16 %
42												16 %
43												17 %
44												17 %
45												17 %
46												18 %
47												20 %
48												18 %

Figure 13. Finer particle (1,0 – 10,2 µm) volume distribution in the estuary by percentage of the total particle volume. Pycnocline represented by the red lines.

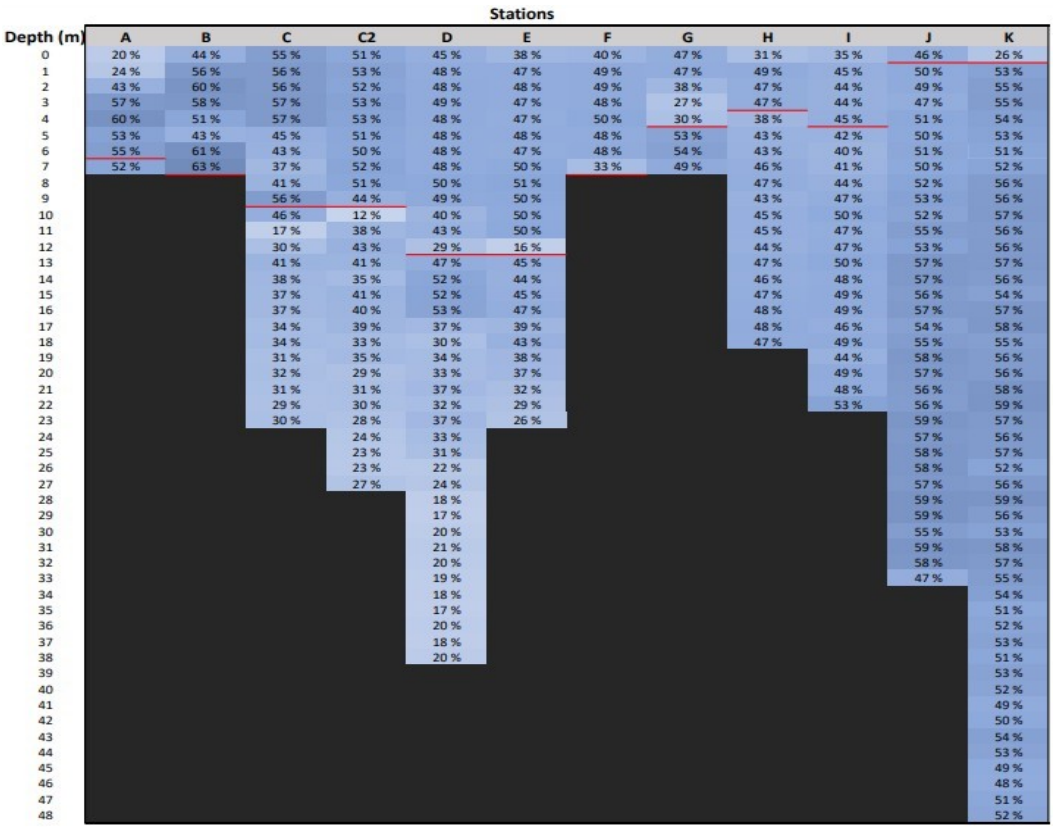

Depth (m)	Stations											
	A	B	C	C2	D	E	F	G	H	I	J	K
0	20 %	44 %	55 %	51 %	45 %	38 %	40 %	47 %	31 %	35 %	46 %	26 %
1	24 %	56 %	56 %	53 %	48 %	47 %	49 %	47 %	49 %	45 %	50 %	53 %
2	43 %	60 %	56 %	52 %	48 %	48 %	49 %	38 %	47 %	44 %	49 %	55 %
3	57 %	58 %	57 %	53 %	49 %	47 %	48 %	27 %	47 %	44 %	47 %	55 %
4	60 %	51 %	57 %	53 %	48 %	47 %	50 %	30 %	38 %	45 %	51 %	54 %
5	53 %	43 %	45 %	51 %	48 %	48 %	48 %	53 %	43 %	42 %	50 %	53 %
6	55 %	61 %	43 %	50 %	48 %	47 %	48 %	54 %	43 %	40 %	51 %	51 %
7	52 %	63 %	37 %	52 %	48 %	50 %	33 %	49 %	46 %	41 %	50 %	52 %
8			41 %	51 %	50 %	51 %			47 %	44 %	52 %	56 %
9			56 %	44 %	49 %	50 %			43 %	47 %	53 %	56 %
10			46 %	12 %	40 %	50 %			45 %	50 %	52 %	57 %
11			17 %	38 %	43 %	50 %			45 %	47 %	55 %	56 %
12			30 %	43 %	29 %	16 %			44 %	47 %	53 %	56 %
13			41 %	41 %	47 %	45 %			47 %	50 %	57 %	57 %
14			38 %	35 %	52 %	44 %			46 %	48 %	57 %	56 %
15			37 %	41 %	52 %	45 %			47 %	49 %	56 %	54 %
16			37 %	40 %	53 %	47 %			48 %	49 %	57 %	57 %
17			34 %	39 %	37 %	39 %			48 %	46 %	54 %	58 %
18			34 %	33 %	30 %	43 %			47 %	49 %	55 %	55 %
19			31 %	35 %	34 %	38 %				44 %	58 %	56 %
20			32 %	29 %	33 %	37 %				49 %	57 %	56 %
21			31 %	31 %	37 %	32 %				48 %	56 %	58 %
22			29 %	30 %	32 %	29 %				53 %	56 %	59 %
23			30 %	28 %	37 %	26 %					59 %	57 %
24				24 %	33 %						57 %	56 %
25				23 %	31 %						58 %	57 %
26				23 %	22 %						58 %	52 %
27				27 %	24 %						57 %	56 %
28					18 %						59 %	59 %
29					17 %						59 %	56 %
30					20 %						55 %	53 %
31					21 %						59 %	58 %
32					20 %						58 %	57 %
33					19 %						47 %	55 %
34					18 %							54 %
35					17 %							51 %
36					20 %							52 %
37					18 %							53 %
38					20 %							51 %
39												53 %
40												52 %
41												49 %
42												50 %
43												54 %
44												53 %
45												49 %
46												48 %
47												51 %
48												52 %

Figure 14. Intermediate particle (10,2 – 103,0 µm) volume distribution in the estuary by percentage of the total particle volume. Pycnocline represented by the red lines.

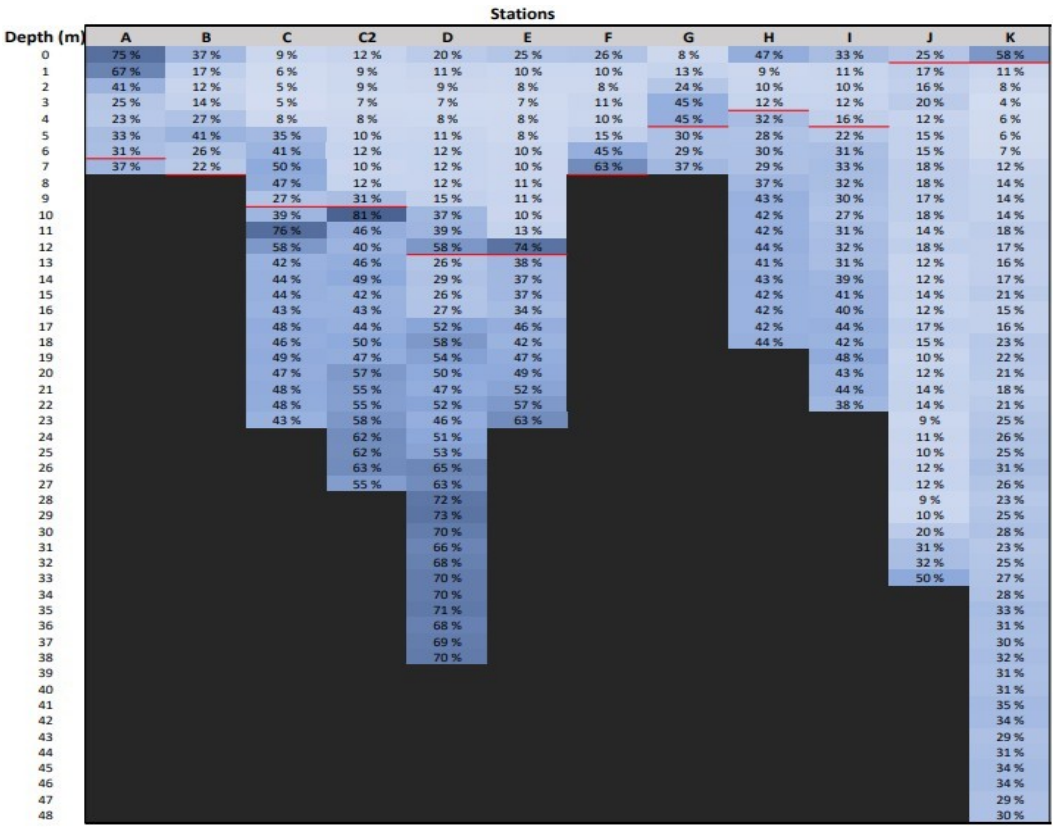

Depth (m)	Stations											
	A	B	C	C2	D	E	F	G	H	I	J	K
0	75 %	37 %	9 %	12 %	20 %	25 %	26 %	8 %	47 %	33 %	25 %	58 %
1	67 %	17 %	6 %	9 %	11 %	10 %	10 %	13 %	9 %	11 %	17 %	11 %
2	41 %	12 %	5 %	9 %	9 %	8 %	8 %	24 %	10 %	10 %	16 %	8 %
3	25 %	14 %	5 %	7 %	7 %	7 %	11 %	45 %	12 %	12 %	20 %	4 %
4	23 %	27 %	8 %	8 %	8 %	8 %	10 %	45 %	32 %	16 %	12 %	6 %
5	33 %	41 %	35 %	10 %	11 %	8 %	15 %	30 %	28 %	22 %	15 %	6 %
6	31 %	26 %	41 %	12 %	12 %	10 %	45 %	29 %	30 %	31 %	15 %	7 %
7	37 %	22 %	50 %	10 %	12 %	10 %	63 %	37 %	29 %	33 %	18 %	12 %
8			47 %	12 %	12 %	11 %			37 %	32 %	18 %	14 %
9			27 %	31 %	15 %	11 %			43 %	30 %	17 %	14 %
10			39 %	81 %	37 %	10 %			42 %	27 %	18 %	14 %
11			76 %	46 %	39 %	13 %			42 %	31 %	14 %	18 %
12			58 %	40 %	58 %	74 %			44 %	32 %	18 %	17 %
13			42 %	46 %	26 %	38 %			41 %	31 %	12 %	16 %
14			44 %	49 %	29 %	37 %			43 %	39 %	12 %	17 %
15			44 %	42 %	26 %	37 %			42 %	41 %	14 %	21 %
16			43 %	43 %	27 %	34 %			42 %	40 %	12 %	15 %
17			48 %	44 %	52 %	46 %			42 %	44 %	17 %	16 %
18			46 %	50 %	58 %	42 %			44 %	42 %	15 %	23 %
19			49 %	47 %	54 %	47 %				48 %	10 %	22 %
20			47 %	57 %	50 %	49 %				43 %	12 %	21 %
21			48 %	55 %	47 %	52 %				44 %	14 %	18 %
22			48 %	55 %	52 %	57 %				38 %	14 %	21 %
23			43 %	58 %	46 %	63 %					9 %	25 %
24				62 %	51 %						11 %	26 %
25				62 %	53 %						10 %	25 %
26				63 %	65 %						12 %	31 %
27				55 %	63 %						12 %	26 %
28					72 %						9 %	23 %
29					73 %						10 %	25 %
30					70 %						20 %	28 %
31					66 %						31 %	23 %
32					68 %						32 %	25 %
33					70 %						50 %	27 %
34					70 %							28 %
35					71 %							33 %
36					68 %							31 %
37					69 %							30 %
38					70 %							32 %
39												31 %
40												31 %
41												35 %
42												34 %
43												29 %
44												31 %
45												34 %
46												34 %
47												29 %
48												30 %

Figure 15. Coarser particle (103 – 200 µm) volume distribution in the estuary by percentage of the total particle volume. Pycnocline represented by the red lines.

3.4 LISST-accuracy assessment

The results from the visual assessment display a general lack of correlation of particle size distribution between the visual rating and the LISST-data (Table 2). There are, however, some exceptions. In station D2, D8, and F0 the ratios of the size fractions are comparable between the visual amount and the LISST-data.

An apparent trend displayed by the results is that the coarse particle fraction is highly underrepresented in the visual assessment (only 1 – 3), compared with the higher share of coarse particles in many stations according to the LISST ratio.

Table 2. The visual volume concentration rating (1 and 10 equal small and high occurrence, respectively) of fine- (1,0 – 10,2 µm), intermediate (10,2 – 103,0 µm) and coarse (103 – 200 µm) particle fractions visually assessed from SEM-pictures compared with the corresponding volume concentration ratios measured by LISST

	Station: C2 10 (1)		Station: C2 10 (2)		Station: D2	
	Visual amount	LISST ratio in %	Visual amount	LISST ratio in %	Visual amount	LISST ratio in %
Fine particle fraction	5	7	6	7	6	43
Intermediate particle fraction	5	12	5	12	5	48
Coarse particle fraction	1	81	1	81	1	9

	Station: D8		Station: D10		Station: D35	
	Visual amount	LISST ratio in %	Visual amount	LISST ratio in %	Visual amount	LISST ratio in %
Fine particle fraction	3	38	3	23	6	11
Intermediate particle fraction	4	50	4	40	4	17
Coarse particle fraction	1	12	1	37	1	71

	Station: E0		Station: F0		Station: G4	
	Visual amount	LISST ratio in %	Visual amount	LISST ratio in %	Visual amount	LISST ratio in %
Fine particle fraction	5	37	5	34	1	25
Intermediate particle fraction	6	38	5	40	3	30
Coarse particle fraction	2	25	3	26	1	45

	Station: H4		Station: J2	
	Visual amount	LISST ratio in %	Visual amount	LISST ratio in %
Fine particle fraction	5	30	3	35
Intermediate particle fraction	4	38	3	49
Coarse particle fraction	3	32	3	16

3.5 Manganese in water columns

The largest concentrations of Mn were found in the estuary. The average Mn concentration in the SWL was around 110 µg/l. The BWL, however, had a larger enrichment especially in the anoxic bottom zone of station D, which had Mn concentrations over 1000 µg/l. The archipelago and the outer sill had generally lower Mn concentrations with values around 60 µg/l (APPENDIX C).

Mn particles below 1 µm, that includes dissolved Mn, comprised over half of the total Mn in the BWL in the estuary; 612 µg/l at the deepest part (Fig. 16). However, insignificant quantities were found in the rest of the transect. Mn particles between 1 – 3 µm were in general poorly represented and had the highest concentration in the SWL in the estuary (Fig. 17). The most common Mn particle size was 3 – 10 µm. These particles were present in both the SWL and BWL in the estuary (Fig. 18). The particles were evenly distributed along the whole transect in concentrations of around 50 µg/l. This particle size was also strongly enriched in the anoxic zone in station D. The largest Mn particles (over 10 µm) were scarce, with the only exception of a small enrichment in the anoxic zone (Fig. 19).

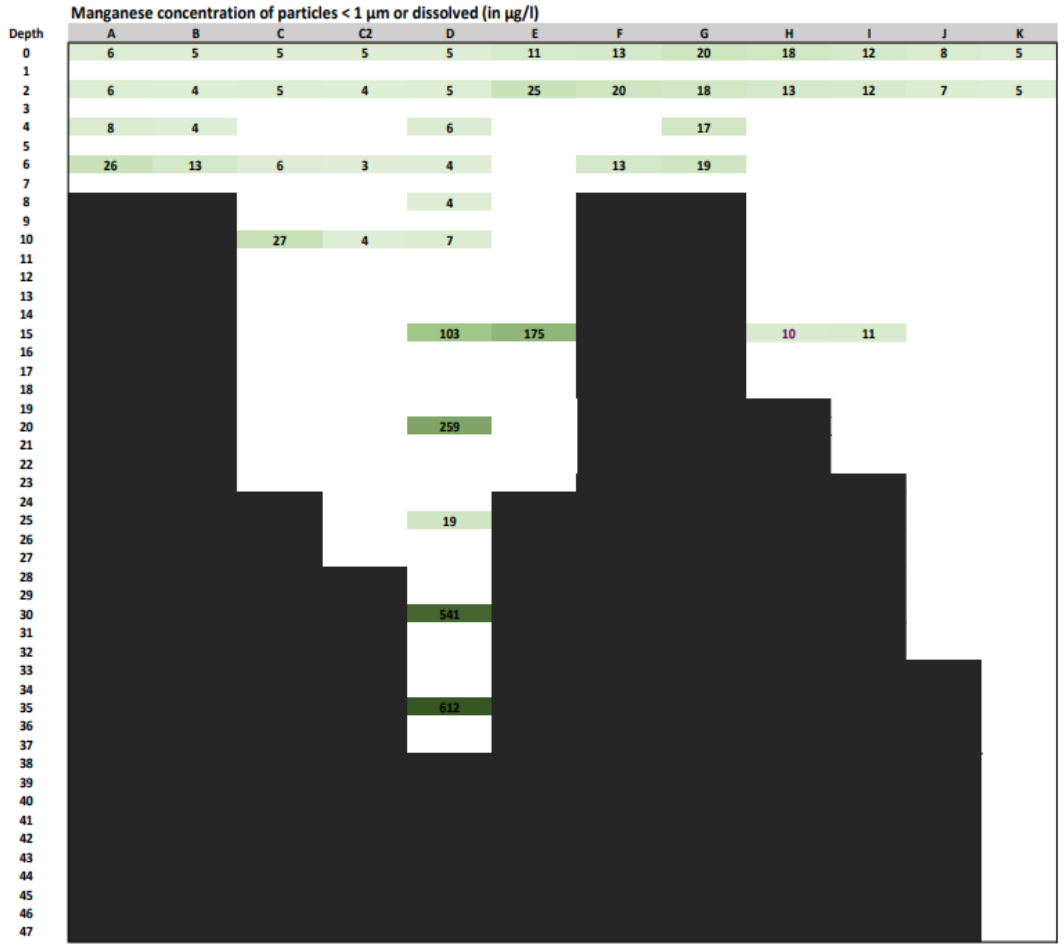

Figure 16. The concentration of Mn-particles (µg/l) under 1 µm, including dissolved Mn, along the estuary in.

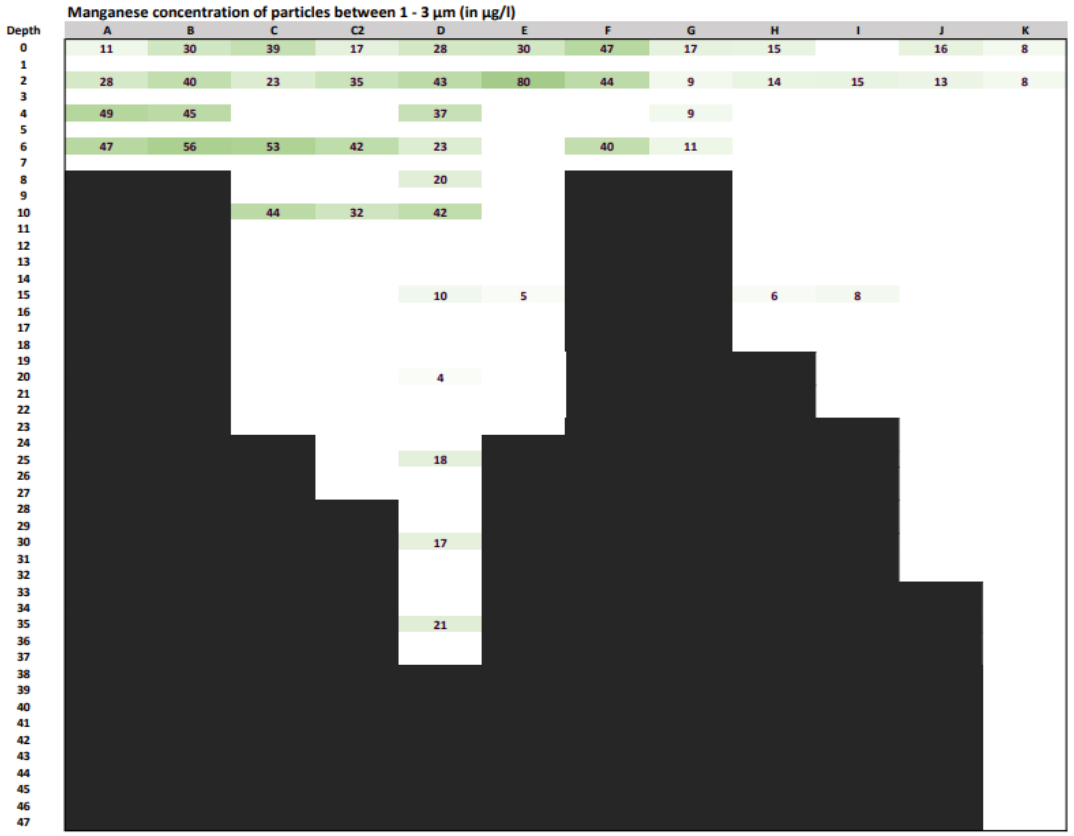

Figure 17. The concentration of Mn-particles between 1 – 3µm along the estuary in µg/l.

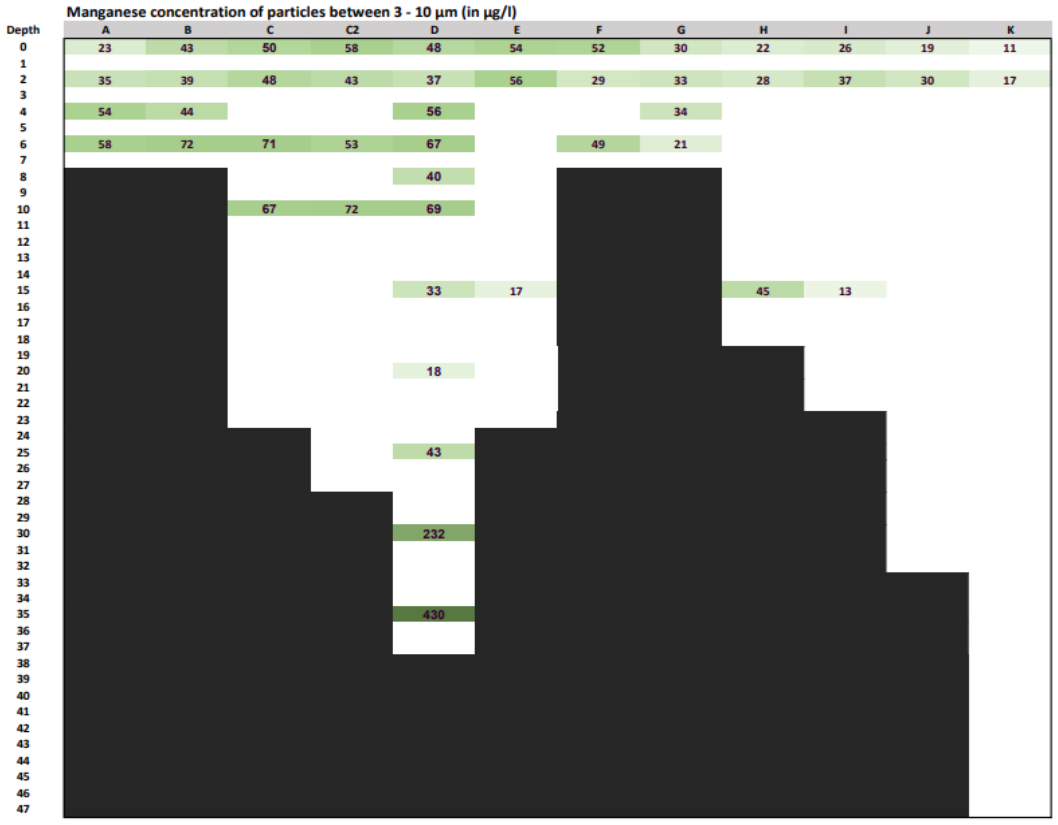

Figure 18. The concentration of Mn-particles between 3 – 10µm along the estuary in µg/l.

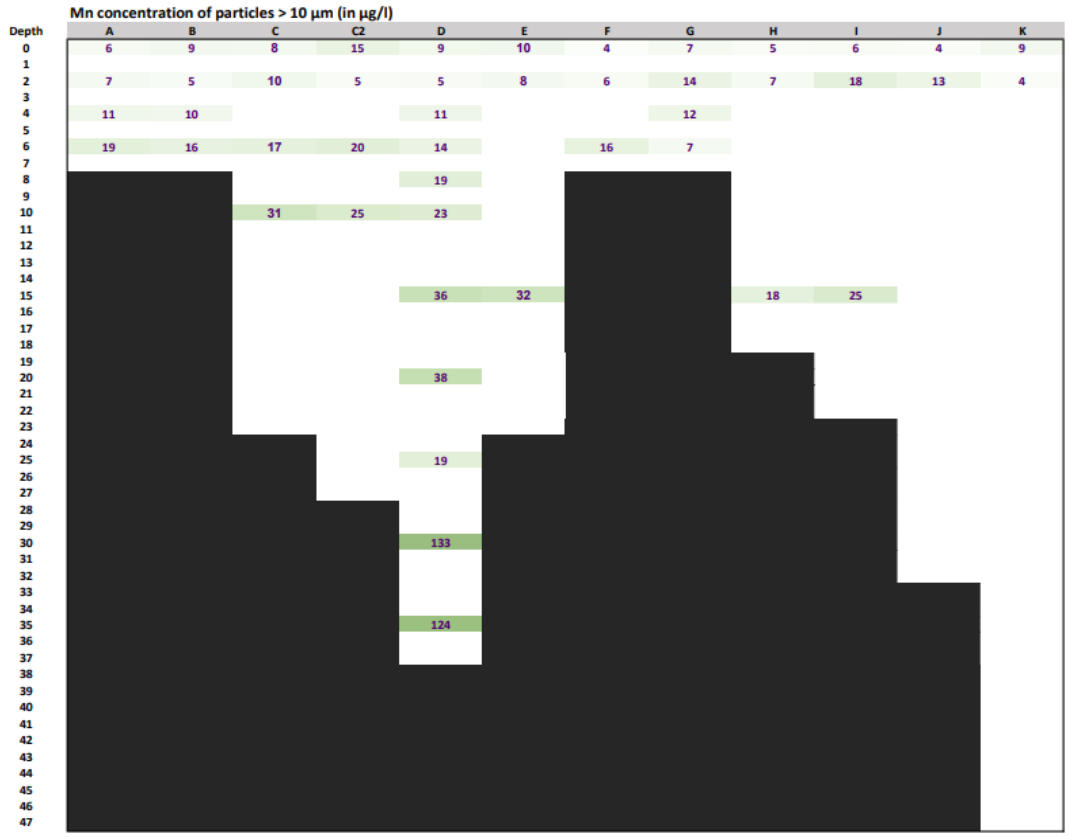

Figure 19. The concentration of Mn-particles > 10µm along the estuary in µg/l.

According to previous particle size definitions (in chapter 3.3), most Mn particles would be defined as finer particles (1,0 – 10,2 µm). However, a comparison between the distribution of finer suspended particles and the concentration of Mn particles along the water column shows that they are unrelatable to each other. In other words, Mn particles make up only a small portion of the total particle pool.

3.6 Particle characterization

The SWL is characterized by finer particles and generally fewer aggregates exceeding 50 µm, with some exceptions near the river mouth at station A and B, where some intermediate to coarser aggregates were present. Further out at stations D and E the SWL contained many smaller particles as well as intermediate aggregates. Coarser organic aggregates and microbes were more represented closer to the sill.

In the estuary under the pycnocline (10 m and deeper) or BWL, there are intermediate amounts of aggregates with sizes over 50 µm.

SEM-pictures from the sill section shows a mixture of all the different particle sizes, but the larger aggregates rarely exceed 100 μm. The upper part (0 – 10 m) of the archipelago was characterized by having excessive coarse organic aggregates, intermediate diatoms and aggregates, as well as finer inorganic particles. The deeper part (under 10m) of the archipelago contained a good number of particles and aggregates. Intermediate and coarser particles and aggregates were most represented at stations H and I, while the aggregates seemed to gently decrease in size further out.

When comparing Mn oxide particles, the SEM-pictures revealed two major particle morphotypes, irregular "star-shaped" (Fig 20) and "cauliflower-shaped" (Fig 21) Mn particles. The star-shaped particles were typically smaller (3 – 5 μm) and were exclusively found in the BWL, with the highest concentration in the near bottom waters in station D (Fig. 20). The cauliflower-shaped Mn particles (Fig. 21) were larger in comparison (5 – 7 μm) and were more scarcely found in oxygenated water along the whole transect.

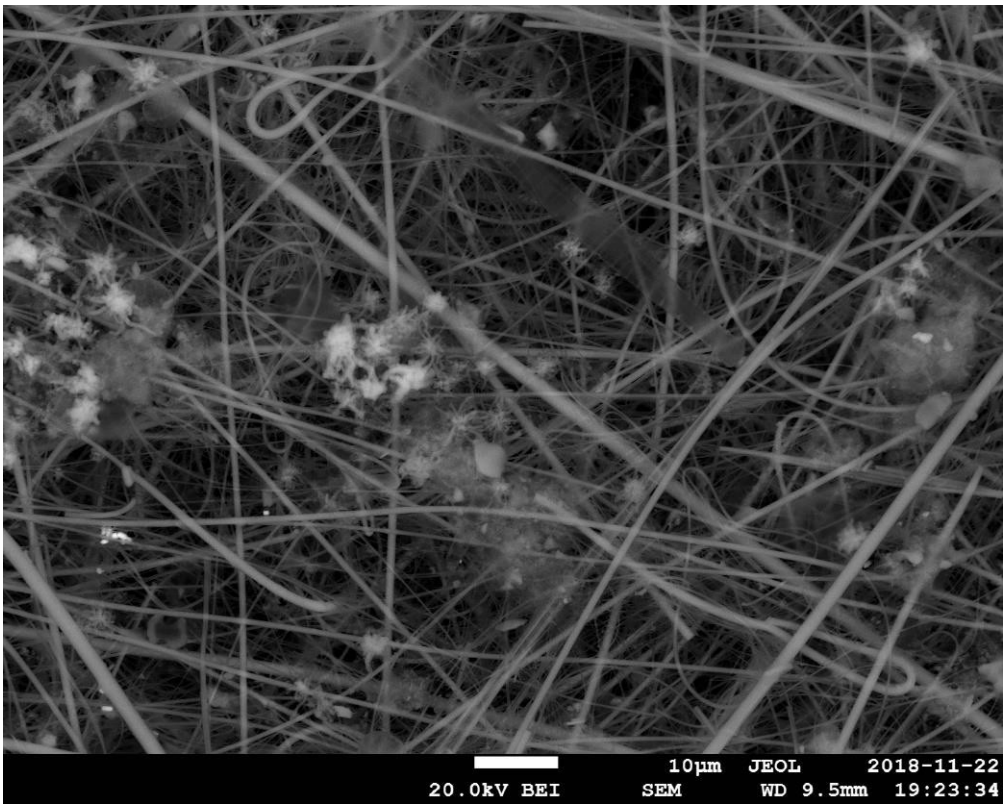

Figure 20. A SEM-picture of retentate received from station D35 showing multiple “star-shaped” Mn particles.

Figure 21. A SEM-picture of retentate received from station D2 showing a “cauliflower-shaped” Mn particle.

4. Discussion

4.1 LISST evaluation

SEM-pictures (with a zoom of x300) were studied, and particle distributions were visually estimated for each size fraction (fine to coarse) by the scale of 1 – 10 (Appendix B). The particle distribution in each size fraction were then compared with the particle distribution of the same fractions from the LISST-data, with the intent to evaluate the accuracy of the LISST-device.

The results of comparing LISST-data with the visual estimations showed that the visual estimations generally have a higher fraction of finer and intermediate particles than coarser particles, whereas the LISST-data generally presents a higher share of coarse particles. The argument behind this result could be an inappropriate size resolution of the SEM-pictures "hiding" larger particles. Another theory is that the LISST-device presumably detects aggregates rather than individual particles, resulting in a higher share of coarse particles. The break-up of these aggregates during filtration and the flattening of the in situ 3D structure of the aggregates on the filters would increase the amount of fine and intermediate particles found in the SEM-pictures, which in return results in higher shares of these particle sizes in the visual assessment. The break-up of soft aggregates during filtration could also be the main reason for the general absence of larger aggregates on the filters. When evaluating the accuracy of the LISST, it is also important to take the validity of the SEM-pictures into account. Due to quality and resolution, few pictures were assessed representing only a tiny fraction of the whole estuary. The pictures themselves were also not taken solely for the visual assessment, but for the SEM-analyzes, in which areas with denser particles were favored. It is hence fair to evaluate the LISST-data as a more reliable source of data compared to the visual assessment method.

Some of the LISST-data in certain stations (D2, D8, and F0) corresponded well with the visual estimations. The result from these stations, however, cannot be used against nor in favor of the accuracy of the LISST because of the reasons mentioned earlier.

Overall, the LISST instrument is an easy and practical tool for measuring particle distribution in marine environments. The fact that the LISST also measures chemical variables is making it a versatile tool for all kinds of marine studies. The instruments have been frequently used in many different applications in marine research. (Graham et al. 2012) (Fugate & Friedrichs, 2002) (Mikkelsen et al., 2006). The advantageous uses of the LISST is therefore outweighing the minor disadvantages.

4.2 The role of seasonal variations on particle distribution

The particle distribution is strongly affected by water circulation cycles in the estuarine transect. The non-tidal *Pohjanpitäjänlahti* estuary receives water-mixing from seasonal variations in the transect. In spring the river discharge is at maximum, adding freshwater from the north decreasing the seawater inflow from the south. In the summer and early autumn, the river discharge is low, causing poor water circulation in the estuary (Niemi, 1977) (Jilbert et al. 2018). Water stagnation in the estuary divides the water into denser water with higher salinity (BWL) in the deeper parts of the estuary, and less dense water (SWL) in the upper part (Fig. 10). Surface water warmed by the sun is thus not mixing between the SWL and the BWL, resulting in a sharper thermocline in the estuary compared to the evenly dense water in the archipelago (Fig. 8). In the winter, however, water temperatures decrease in the SWL simultaneously as an increased inflow of sea water due to a minimum river discharge, causing an improvement in water circulation in the estuary (Virta, 1977).

The enrichment of SP near the river mouth is caused by transported erosional matter from the catchment-area. The majority of SP from the river outlet may settle towards the next stations. The Pycnocline, which is the interface between lighter (less salty) and heavier (saltier) water (Fig. 10) is working as a physical barrier, which delays the settling of SP concentrating them along the pycnocline. Enrichment of SP causes particle aggregation along the pycnocline (Petros, 2017), resulting in a higher concentration of courser particles (Fig. 15). The high near-bottom values of particle volume concentration (> 140ml/l) in station F and J can be caused due to high resuspension, especially in station F where the topography

drastically changes (Fig. 12). The high values can, however, also be a result of the LISST-instrument hitting the bottom.

4.3 The redox-driven cycling of manganese

Increased growth of phytoplankton in the summer simultaneously increases the microbial decomposition processes of sedimented organic compounds. The decomposition processes consume dissolved oxygen in the water, leading to oxygen depletion. In combination with water stagnation, oxygen depletion increases in the deeper parts (BWL) of the estuary (C2 – E). As a result, redox conditions are formed on the bottom, which is having impact on the redox-sensitive Mn.

In reduced environments sedimented Mn-oxides are easily used as an electron acceptor by metal-reducing bacteria, reducing Mn (III, IV) oxides to dissolved Mn (II) in sediments. Dissolution of Mn (II) in the sediments is then causing Mn (II) to be transported by bottom turbidity into the near bottom water, resulting in high concentrations of dissolved Mn in the lower water column, as seen in station D (Table 10). In the presence of oxygen, microorganisms contribute to the oxidation of Mn (II), forming Mn (III, IV) oxides in the water column, which are later re-sedimented (Sunda & Huntsaman, 1990; Neretin et al. 2003; Tebo et al. 2004). By these redox processes Mn is cycled up and down within the bottom sediments and BWL in the process which can be referred to as “Mn shuttling” (Jilbert et al. 2018). Because of a seemingly low redox potential in the bottom waters the Mn (II) / Mn (III, IV) ratio is higher, especially in the deeper part of station D, resulting in a higher concentration of dissolved Mn.

4.4 Manganese distribution and formations

Considering the processes of Mn shuttling in the BWL, it is easier to explain the remaining distribution of the solid Mn particles along *Pohjanpitäjänlahti* estuary. Mn particles originates from the catchment area and are carried via the Mustinjoki river to the estuary, where the particles are transported along the water column in the SWL, trough the sill section and out in the archipelago. Because of the elevated Mn concentrations in the near bottom waters in the BWL, an accumulation of Mn particles derived from the overlying SWL should be logical (Appendix C). The Mn

distribution results show that some Mn particles settle trough the pycnocline, but these are mainly coarser particles (> 3 μm) (Fig 16 - 18). It is, however, important to consider Mn particles as parts of larger aggregates (> 103 μm), which is more prone to settle trough the pycnocline.

SEM-pictures of Mn particles show that the particles from the BWL differ in shape and size from the particles in the SWL. In the hypoxic BWL, the Mn particles are shaped as irregular stars (Mn stars) with a diameter of 3 – 5 μm. In the SWL, Mn particles are instead shaped as cauliflowers (Mn cauliflowers) and have a slightly larger diameter (5 – 7 μm). The suspended Mn cauliflowers are most likely derived from the catchment area and is transported with the current along the surface water of the estuary. The Mn stars, however, are formed through redox processes in the hypoxic BWL in the estuary. These particles are drawn upward in the water column, but since the inner estuary is characterized by a strong (seasonal) pycnocline that prevents mixing of the SWL and BWL, Mn stars do not reach the surface waters. Instead the Mn stars settle again and repeat the process (Mn shuttling). It is possible that lower contents of Mn in the oxic zone lead to a slower and more developed nodule structure than in the Mn rich anoxic zone where even soluble Mn is expected to be found. This finding suggest that the Mn particles have different origins, which would be an important part in understanding the Mn cycling in the estuary. This theory would also explain why the two Mn morphotypes are not seen simultaneously in the SEM-pictures.

5. Conclusion

The distribution of suspended particles (SP) along the *Pohjanpitäjänlahti* estuary is largely influenced by physical and chemical variables in the water column. SP were mostly concentrated near the river mouth, along the pycnocline (with some exceptions in D and E), and at deeper parts of the stations from the sill section to the archipelago. The size fraction distribution of the particles showed that finer particles dominated surface layers of the water column, while coarser particles tended to dominate the deeper parts.

Poor water circulation causes the water in the estuary to divide into a surface water layer (SWL) and a bottom water layer (BWL) at the depth of about 12 m. Combined with higher decomposing processes in the sediments, the poor water circulation ultimately leads to hypoxic/anoxic conditions in the BWL. The lack of oxygen decreases the redox potential, dissolving Mn in the sediments. Dissolution of Mn in the sediments increases the concentration of Mn in the bottom waters. When in contact with more oxygenated water, microorganisms assist in oxidization of dissolved Mn, precipitating it. The precipitated Mn-particles may then travel by turbidity up the BWL until they take part in aggregation at the pycnocline, which results in re-sedimentation of the heavier aggregates. This redox-driven process of Mn-cycling can also be referred to as Mn-shuttling.

Mn particles found in the SEM analyzes displayed two major morphotypes of Mn-oxides, star-shaped (Mn stars), and cauliflower-shaped (Mn cauliflowers) particles. Mn stars were exclusively found in the hypoxic zone in the estuary, while Mn cauliflowers were mostly found along the surface. The different morphotypes indicates different origins of the particles, with Mn stars formed by the Mn-shuttling in hypolimnion and Mn cauliflowers originating from the catchment area.

The visual assessment of particle characterization on SEM-pictures generally indicated a higher share of finer particles than the LISST instrument. The assessment failed to prove nor disprove the accuracy due to the shortage of qualitative SEM-pictures, and dividing particle referencing. However, the LISST instrument probably gives a more realistic estimate of the in-situ 3D geometry of

the particles than the broken-up and flattened particles on the filter surface. The LISST is furthermore a good and user-friendly tool that also provides necessary additional water data and is hard to replace in terms of effectiveness.

Aknowledgements

I would like to express my deepest gratitude to my supervisors Peter Österholm and Joonas Virtasalo for providing guidance and expertise during the whole work process. Without your help, patience, and inspiration this thesis would not have seen the light of day.

A special thank you to Tom Jilbert and Eero Asmala for providing useful data and consultation along the way. I would also like to thank Matias Scheinin, Sara Newton, and the crew on R/V Geomari for their cooperation during the sampling trip.

I will also turn my gratitude towards my wife Elin as well as my friends and family for giving me mental support during the writing process, thank you all.

Finally, I want to thank the Geohouse staff at Åbo Akademi University and University of Turku for their availability and support during my time at the university.

Swedish summary

Distribution och karaktärisering av suspenderade partiklar i Pojovikens estuarium

Introduktion

Suspenderade partiklar (SP) förekommer i naturliga vattendrag, sjöar och hav. En partikel kan bestå av ett urval av material från lera och kemiska fällningar till biogena partiklar som fytoplankton, kiselalger, växtalger och kolloidal humus. Oorganiska partiklar i vattenmassor härrör vanligtvis från berggrunden och marken i avrinningsområdet. När SP kolliderar med varandra i vattenkolumnen kan de bindas till större aggregat (Maggi, 2005). Större och tyngre aggregat som innehåller silikater och metalliska fällningar sjunker till havsbotten där de sedimenteras. SP kan även bindas eller fällas ut genom kemisk attraktion, detta kallas flockulation (Van Leussen, 1988). Flockulation är vanlig vid flodmynningar där sött åvatten blandas med salt havsvatten (Asmala et al, 2014). Efter sedimentation kan partiklar och aggregat återgå till suspension genom fysikaliska och kemiska processer.

Mangan (Mn) är en av de vanligaste metallerna i jordskorpan och återfinns som huvudelement i många mineralkonfigurationer. Mangan är ett mobilt ämne som enkelt transporteras från berg och mark till floder, sjöar och hav (Post, 1999). Redoxförhållanden i och ovanför bottensediment inverkar på de processer som löser upp och fäller ut mangan, och har därmed en viktig roll i uppdelningen av löst och partikelformigt (fast) mangan i sjöar och estuarier (Sunda & Huntsaman, 1990). Tillsammans med järn (Fe) kan reducerat Mn oxideras och fällas ut med fosfatjoner, vilket minskar på löst fosfat i vattenkolumnen. Eftersom den lösta fosfaten upptas av växtlighet motverkar Mn och Fe oxidationen eutrofiering (Gaosheng et al. 2009).

Pojovikens estuarium är belägen i kommunerna Raseborg och Hangö i södra Finland (Fig. 1). I norra delen av estuariet tillför Svartån sötvatten, som gradvis blandas ut med havsvatten söderut mot Finska viken. Pojovikens estuarium kan delas in i tre sektioner utgående från fysikaliska och geografiska egenskaper. Estuariet är den nordligaste sektionen som karaktäriseras av en större andel sötvatten. Det åtföljs av en mellansektion, som är en smalare och grundare del av Pojovikens estuarium. Efter mellansektionen kommer skärgårdsestuariet, som är den sydligaste sektionen med utlopp i Finska viken. Mellan Svartåns mynning i norr till den sista provpunkten (Station K) i Finska viken är distansen ca 30 km, medan bredden längs hela estuariet är mellan 0,2 - 3 km (Fig. 1) (Tiihonen, 2016).

Proverna som behandlas i denna avhandling har samlats in från tolv provtagningsstationer (A - C, C2, D - K) längs hela studieområdet (Fig. 1). Estuariet utgörs av stationerna A - C, C2, D och E, mellansektionen utgörs av stationerna F och G och skärgårdsestuariet utgörs av stationerna H - K. Stationerna besöktes med forskningsfartyget R/V Geomari under hösten 2018.

Syfte

Denna avhandling har tre huvudmål. Det första målet är att kvantifiera och karaktärisera suspenderade partiklar (SP) längs Pojovikens estuarium. Det andra målet är att förstå den redox-drivna Mn-cykeln i estuariet. Det tredje målet är att förevisa användningen av en *LISST*-partikelstorleksanalysator inom marin forskning.

Material och metod

De fysikaliska och kemiska egenskaperna i Pojovikens estuarium mäts av en *YSI EXO2*-multiparametersond och en *Sea & Sun Technology CTD 90 M Series II* multiparameter sond. De viktigaste parametrarna som mäts är temperatur, tryck, koncentrationen av löst syre, pH och turbiditet. Ett *Sequoia LISST-100X* multiparameter (LISST) instrument används för att mäta fördelningen och koncentrationen av SP-storlekar i vattenkolumnen längs hela studieområdet. För att korrelera data, fästs samtliga instrument på en stålram, som sänks från vattenytan till botten med hjälp av en vajerkran på fartyget (Fig. 3).

Vattenprover tas från specifika djup vid varje station. Orsaken bakom vattenprovtagning är att fastställa massan och volymkoncentrationen av SP vid olika djup längs estuariet. Provtagningen sker *in situ* med en Limnos-provtagare som rymmer 2,5 liter (Fig. 4). Vattenprov från varje station förvaras sedan i 0,5 liters plastflaskor. En uppmätt mängd vatten (300 ml) filtreras senare genom *Whatman* 0,7 µm-filter. Efter filtrering frystorkades filtren för att kunna genomföra ytterligare analyser.

Totalt 35 filter valdes ut för analys med ett svepelektronmikroskop (SEM). Med SEM undersöktes enstaka partiklar och aggregat på filtren med hjälp av elektrondispersiv röntgenspektroskopi (EDS). Genom EDS-analys kan sammansättningen av utvalda partiklar på filtren bestämmas. Huvudorsaken bakom EDS-analysen är att hitta samt karakterisera eventuella Mn-partiklar på filtren. För att senare jämföra Mn-partiklar tas även bilder på mikroskala över eventuella fynd under SEM-analysen.

I en parallell studie med samma vattenprov utfördes filtrering i tre steg. En bestämd mängd vatten filtrerades först genom ett *Whatman* 10 µm-filter, varpå vattnet igen filtrerades, denna gång genom ett *Whatman* 3,0 µm-filter. Slutligen filtrerades residualvattnet en tredje gång genom ett *Whatman* 1,0 µm-filter (Newton, 2019). Genom denna process koncentrerades SP över 10 µm på första filtret, SP mellan 3 och 10 µm på andra filtret och SP mellan 1 och 3 µm på tredje filtret. SP under 1 µm samt lösta joner sparades i residualvattnet. Filtren blev sedan upplösta i syra och analyserade med induktivt kopplad plasma - masspektroskopi (ICP-MS), medan residualvattnet analyserades med induktivt kopplad plasma - atomstrålningsspektroskopi (ICP-OES). Analyserna gjordes för att klarlägga koncentrationen av Mn i olika partikelstorlekar samt koncentrationen av löst Mn i vattenkolumnen längs estuariet.

För att verifiera noggrannheten på LISST instrumentet gjordes en visuell bedömning av utvalda SEM-bilder. Genom att visuellt bedöma koncentrationen mellan storleksfraktionerna fin- (1,0 – 10,2 µm), medel- (10,2 – 103,0 µm) och grovkornig (103 – 200 µm) kan man senare jämföra resultatet med LISST-resultatet över samma storleksfraktioner.

Resultat och diskussion

På basis av temperatur och salinitetsvärden (Fig. 8 – 9) kan man ange vattendensiteten längs estuariets vattenkolumn (Fig. 10). I detta fall (hösten 2018) är vattendensiteten högst (1005 g/l) i skärgårdsestuariet. Orsaken till detta är att en högre salthalt i havsvattnet (Fig. 9) bidrar till en högre densitet. I mellansektionen minskar densiteten från 1005 g/l vid station G, till 1002 g/l vid station D (Fig. 10). Vid dessa stationer blandas sötare åvatten från norr och saltare havsvatten från söder (Fig. 9). Varmare och sötare vatten (1,002 g/l) bidrar till en tydlig densitetsskillnad mellan övre och undre skiktet (ca 1,004 g/l) i estuariet (Fig. 8). Estuariet kan djupledes delas in i ett ytvattenskikt (YVS) och ett bottenvattenskikt (BVS), eftersom vattendensiteten skiljer dessa åt på ett djup mellan 6 – 12 m. Gränsen mellan dessa skikt kallas för pyknoklin. I BVS var temperaturen lägre på grund av dålig vattencirkulation mellan det varmare YVS (Fig. 8). Syrehalterna var i allmänhet goda genom hela estuariet (cirka 10 mg/l), förutom i BVS i estuariet, som hade hypoxiska värden mellan 1 - 2 mg/l. I de djupaste delarna av station D (34 - 37 m) rådde ett anoxiskt tillstånd (Fig. 11).

LISST-data visar fördelningen av partiklar i storleksintervallet 1,00 - 200 µm och deras volymkoncentration i mg / l. Partiklarna delades in i storleksfraktionerna finkorniga partiklar (1,0 – 10,2 µm), medelstora partiklar (10,2 – 103,0 µm) och grovkorniga partiklar (103 – 200 µm). Storleksfraktionernas procentuella volymandel beräknades därefter ut för att karaktärisera partikeldistributionen av fin-, medel- och grovkorniga partiklar längs hela studieområdet (Fig. 13 – 15). Finkorniga partiklar har (i förhållande till de andra fraktionerna) sin största procentuella andel i estuariets YVS (Fig. 13), medan grovkorniga partiklar är i majoritet kring pyknoklinen och i BVS (Fig. 15). Orsaken till detta är att grövre partiklar ofta har en snabbare sedimentationshastighet, medan finkorniga partiklar har en längre suspensionstid. Detta fenomen gäller även i skärgårdsestuariet där grovkorniga partiklar anrikas på djupet medan finkorniga partiklar utgör den största andelen i ytvattnet. Medelkorniga partiklar har till skillnad från de övriga fraktionerna en jämn fördelning längs hela estuariet (Fig. 14).

Den visuella bedömningen av SEM-bilderna visade en dålig korrelation mellan resultatet av bedömningen och det uppmätta resultatet från LISST instrumentet (Tabell. 2). I den visuella bedömningen utgjorde finkorniga partiklar en större andel än de grovkorniga partiklarna i jämförelse med LISST-resultatet. Orsaken till de olika resultaten kan bero på att LISST instrumentet registrerar aggregat som grova partiklar, vilket ökar andelen av dessa i LISST-resultatet. Tvärtemot LISST-resultatet går de grova aggregaten sönder under filtreringsprocessen, vilket resulterar i en mindre andel grovkorniga partiklar observerade i den visuella bedömningen (Appendix B).

Mn-koncentrationen är högst i estuariet (runt 100 µg/l) och lägst i skärgårdsestuariet (runt 70 µg/l) (Appendix C). De högsta Mn-halterna finns i estuariets BVS, särskilt på de djupaste ställena med hypoxiska till anoxiska tillstånd (station D), med koncentrationer upp emot 1100 µg/l. På grund av redoxmiljöer i BVS utgörs över hälften av Mn-koncentrationen där av upplöst Mn (reducerat Mn (II)), medan andelen upplöst Mn är obetydlig i resterande delar av studieområdet (Fig. 16). Mn-partiklar över 10 µm utgör en mycket liten andel av den totala koncentrationen och är i huvudsak anrikade i djupare delar av station D (Fig. 19). Mn-partiklar mellan 3 och 10 µm är även de anrikade i de djupare delarna av station D (Fig. 18), men utgör också tillsammans med partikelstorlekarna 1 – 3 µm (Fig. 17) största delen av Mn-koncentrationen längs de resterande delarna av studieområdet.

SEM-bilder av Mn-partiklar visar att partiklarna från BVS skiljer sig i form och storlek från partiklarna i YVS. I de syrefattiga BVS är Mn-partiklarna formade som oregelbundna stjärnor (Fig. 20) med en diameter på omkring 4 µm. I YVS är Mn-partiklar (~6 µm) istället formade som kålhuvudliknande klot (Fig. 21). Orsaken till formskillnaden har att göra med Mn-partiklarnas olika ursprung. Mn-klot härstammar troligtvis från avrinningsområdet och transporteras med strömmen längs ytvattnet i estuariet. Mn-stjärnor bildas i motsats till de större kålhuvudformade Mn-partiklarna genom redoxprocesser i den syrefattiga bottendelen av estuariet. I normala fall dras en del av dessa partiklar uppåt i vattenkolumnen med hjälp av turbiditetsströmmar, men eftersom estuariet karaktäriseras av en stark pyknoklin som förhindrar blandning av YVS och BVS, kommer Mn-stjärnor inte upp till ytvattnet. Mn-stjärnorna sedimenterar därför igen och upprepar processen. Denna teori skulle förklara de höga Mn-koncentrationerna i BVS.

Den totala partikelstorleksfördelningen längs estuariet går inte att korrelera till Mn-partiklarnas storleksfördelning, eftersom proportionerna kraftigt skiljer sig. Majoriteten av Mn-partiklarna faller inom storleksramen för finkorniga partiklar.

References

Asmala E., Bowers D. G., Autio R., Kaartokallio H., Thomas D. N. (2014). *Qualitative changes of riverine dissolved organic matter at low salinities due to flocculation.* Journal of Geophysical Research: Biogeosciences. AGU Publications. 15 p.

Fugate D. C. & Friedrichs C. T. (2001). *Determining concentration and fall velocity of estuarine particle populations using ADV, OBS and LISST.* Continental Shelf Research 22 (2002). Pp 1867–1886

Gaosheng Z., Huijuan L., Ruiping L. Jiuhui Q. (2009). *Removal of phosphate from water by a Fe-Mn binary oxide adsorbent.* Journal of Colloid and Interface Science 335. Pp 168 – 174. Elsevier.

Gill A. E. (1982). *Atmosphere – Ocean Dynamics.* Academic Press. University of Cambridge. 681 p.

Goldstein J. I., Newbury D. E., Echlin P., Joy D. C., Romig A. D. Jr., Lyman C. e., Fiori C., Lifshin E. (1992). *Coating and Conductivity Techniques for SEM and Microanalysis.* Pp 671. Springer, Boston. MA.

Goldstein J. I., Newbury D. E., Michael J. R., Ritchie N. W. M., Scott J. H. J., Joy D. C. (2018). *Scanning Electron Microscopy and X-Ray Microanalysis.* Fourth Edition. Springer. 226 p.

Graham G. W., Davies E. J., Nimmo-Smith W. A. M., Bowers D. G., Braithwaite K. M. (2012). *Interpreting LISST-100X measurements of particles with complex shape using digital in-line holography.* Journal of Geophysical Research, Vol 117. C05034. 20 p.

Hein J. R., Koschinsky A., Halbach P., Manheim F. T., Bau M., Kang J-K., Lubick M. (2016). *Iron and manganese oxide mineralization in the Pacific.* Pennsylvania State University. 16 p.

Jilbert T., Asmala E., Schröder C., Tiihonen R., Myllykangas J-P., Virtasalo J. J., Kotilainen A., Peltola P., Ekholm P., Hietanen S. (2018). *Impacts of*

flocculation on the distribution and diagenesis of iron in boreal estuarine sedimens. Biogeosciences, 15. Pp 1243–1271

Maggi F. (2005). *Flocculation dynamics of cohesive sediment.* Delft University of Technology. 154 p. PrintPartners Ipskamp B.V., The Netherlands

Mikkelsen O. A., Hill P., Milligan T. G. (2006). *Single-grain, microfloc and macrofloc volume variations observed with a LISST-100 and a digital floc camera.* Journal of Sea Research, 55 (2). Pp 87 – 102.

Newton S. (2019). *Effects of salt induced flocculation on biogeochemical transformation of nutrients in estuarine environments.* University of Helsinki. 43 p.

Neretin L.N., Pohl C., Jost G., Leipe T., Pollehne F., (2003). *Manganese cycling in the Gotland Deep, Baltic Sea.* Marine Chemistry, volume 82, issues 3-4. Pp 125 – 143.

Niemi Å. (1977). *Hydrography and Oxygen Fluctuations in Pojoviken, Southern coast of Finland, 1972 - 1975.* Institute of Marine Research. Helsinki. Pp. 23 – 35.

Petros P. (2017). *Particle size dynamics of suspended particulate matter in Pohjanpitäjänlahti: A LISST-100X campaign.* University of Helsinki. 58 p.

Post J. E., (1999). *Manganese oxide minerals: Crystal structures and economical and environmental significance*. National Academy of Science. Vol 96. Pp 3447 – 3454.

Sequoia (2020). LISST-100X. Sequoia official webpage: http://www.sequoiasci.com/product/lisst- 100x/

Sunda W. G., Huntsman S. A., (1990). *Die1 cycles in microbial manganese oxidation and manganese redox speciation in coastal waters of the Bahama Islands.* American Society of Limnology and Oceanography, Inc. Vol 35. Pp 325 – 338.

Tebo B.M., Bargar J.R., Clement B.G., Dick G.J., Murray K.J., Parker D., Verity R. and Webb S. M. (2004). *Biogenic manganese oxides: Properties and mechanisms of formation*. Annual Review of Earth and Planetary Sciences 32. Pp 287–328.

Tiihonen R. (2016). *The distribution of iron and manganese in coastal sediments of the Gulf of Finland.* Master of Science Thesis. University of Helsinki. Department of Geosciences and Geography. 68 p.

Van Leussen W. (1988). *Aggregation of Particles, Settling Velocity of Mud Flocs A Review*. Physical Processes in Estuaries. Springer-Verlag Berlin Heidelberg. Pp 347 – 551.

Virta J. (1977). *Estimating the Water and Salt Budgets of a Stratified Estuary.* University of Helsinki. Nordic Hydrology, 8. Pp 11 – 32.

YSI (2020). EXO2 multiparameter sonde. YSI official webpage: https://www.ysi.com/EXO2

APPENDICES

Appendix A: Longitudinal section of the Pohjanpitäjänlahti estuary

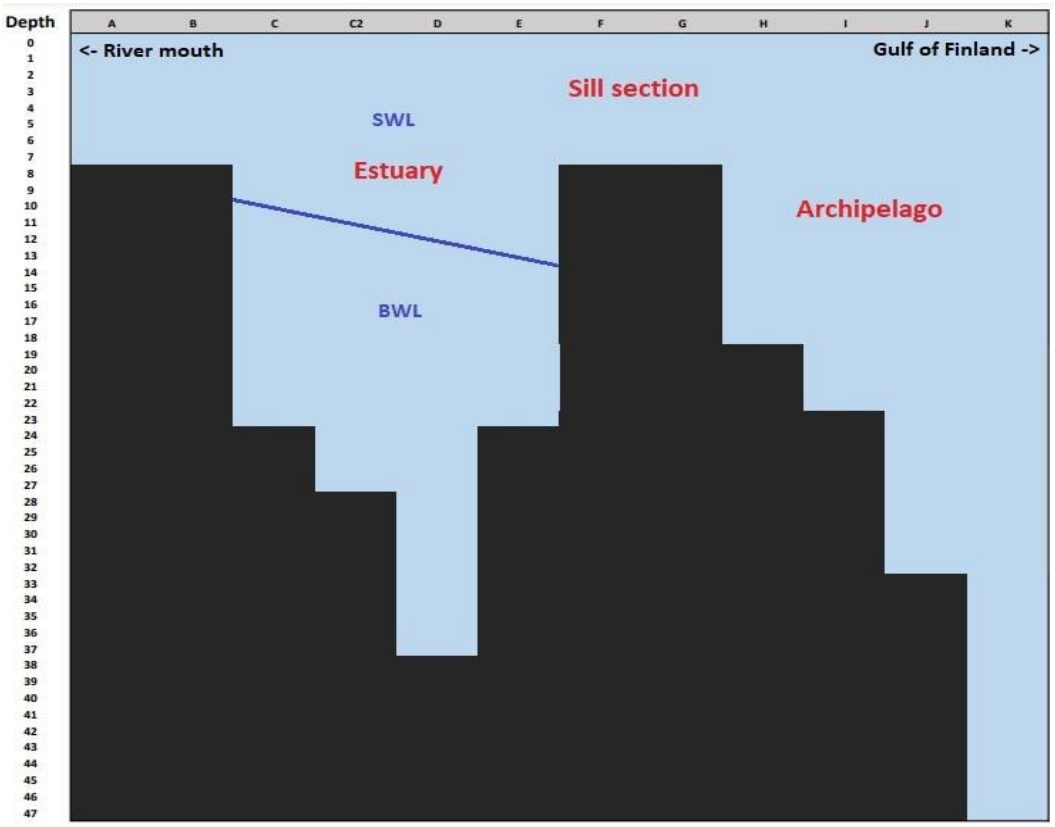

Figure A1. Sections of the *Pohjanpitäjänlahti* estuarine transect.

Appendix B: Visual particle assessment

Station: C2 10 (1) Visual fraction: 5/5/1 LISST-100X fraction (in %): 7/12/81

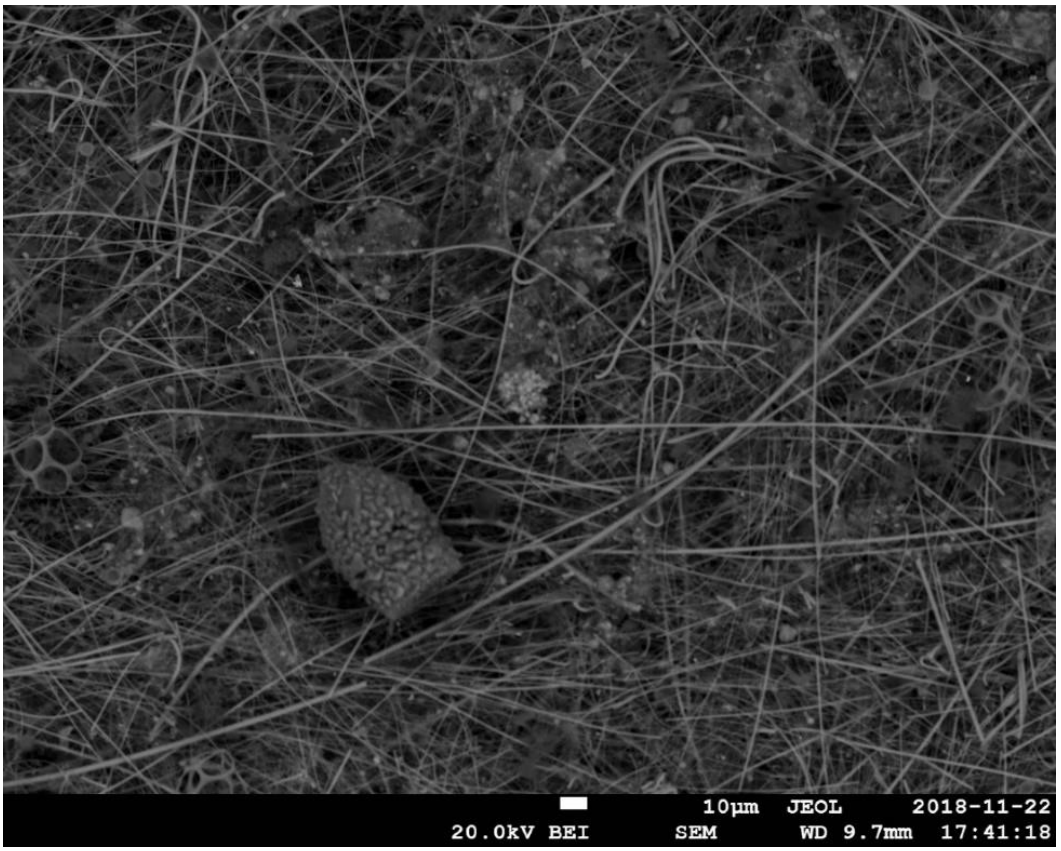

Figure B1. Fraction: Fine/Intermediate/Coarse (amounts in scale 1 – 10).

Station: C2 10 (2) Fraction: 6/5/1 LISST-100X (in %): 7/12/81

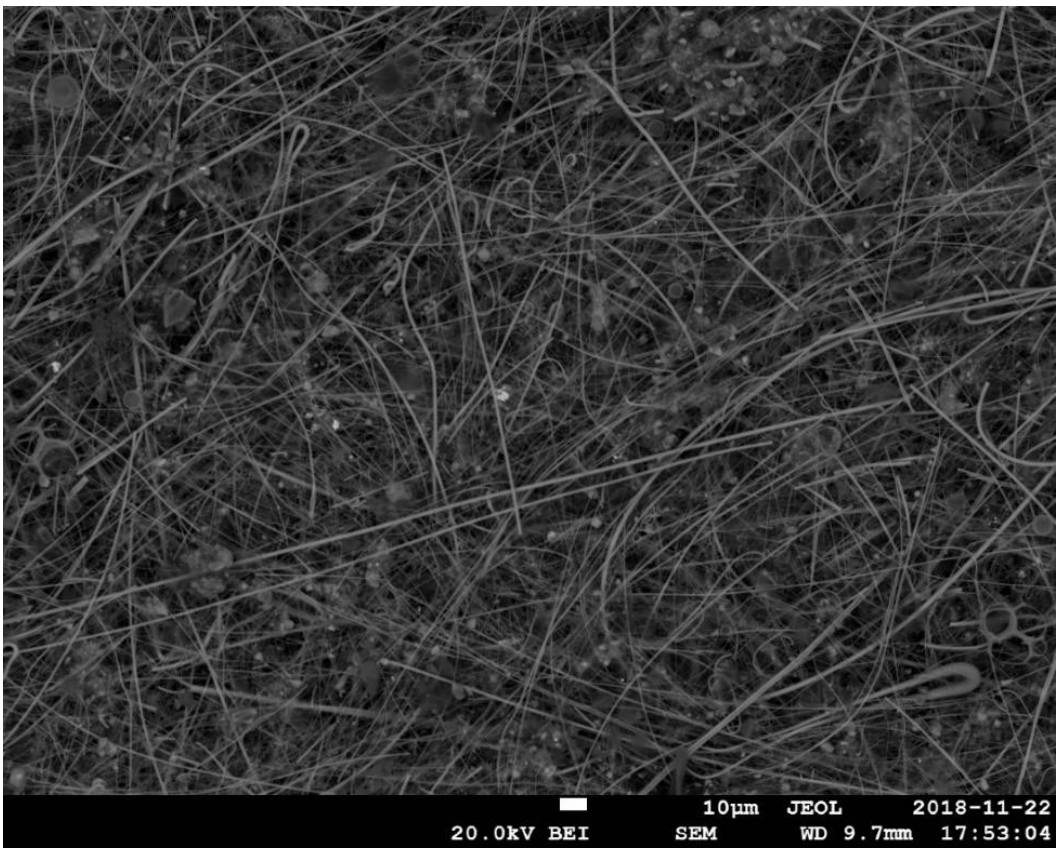

Figure B2. Fraction: Fine/Intermediate/Coarse (amounts in scale 1 – 10).

Station: D2 Fraction: 6/5/1 LISST-100X (in %): 43/48/9

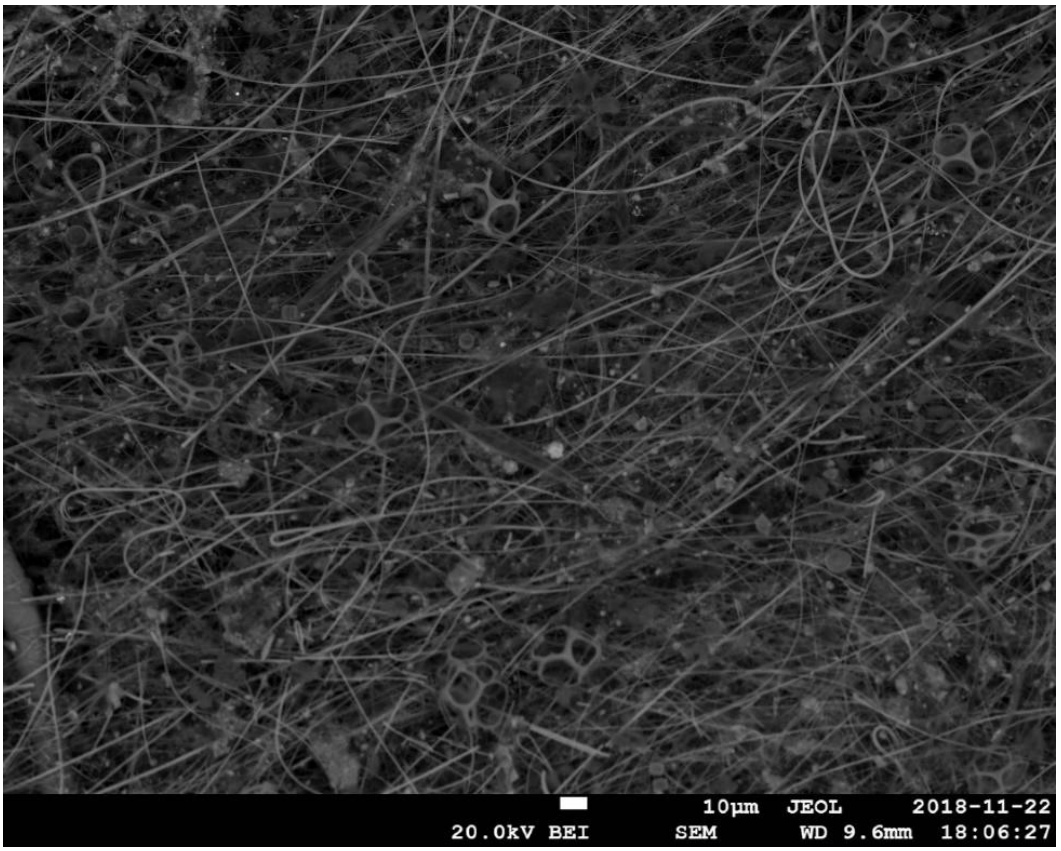

Figure B3. Fraction: Fine/Intermediate/Coarse (amounts in scale 1 – 10).

Station: D8 Fraction: 3/4/1 LISST-100X (in %):38/50/12

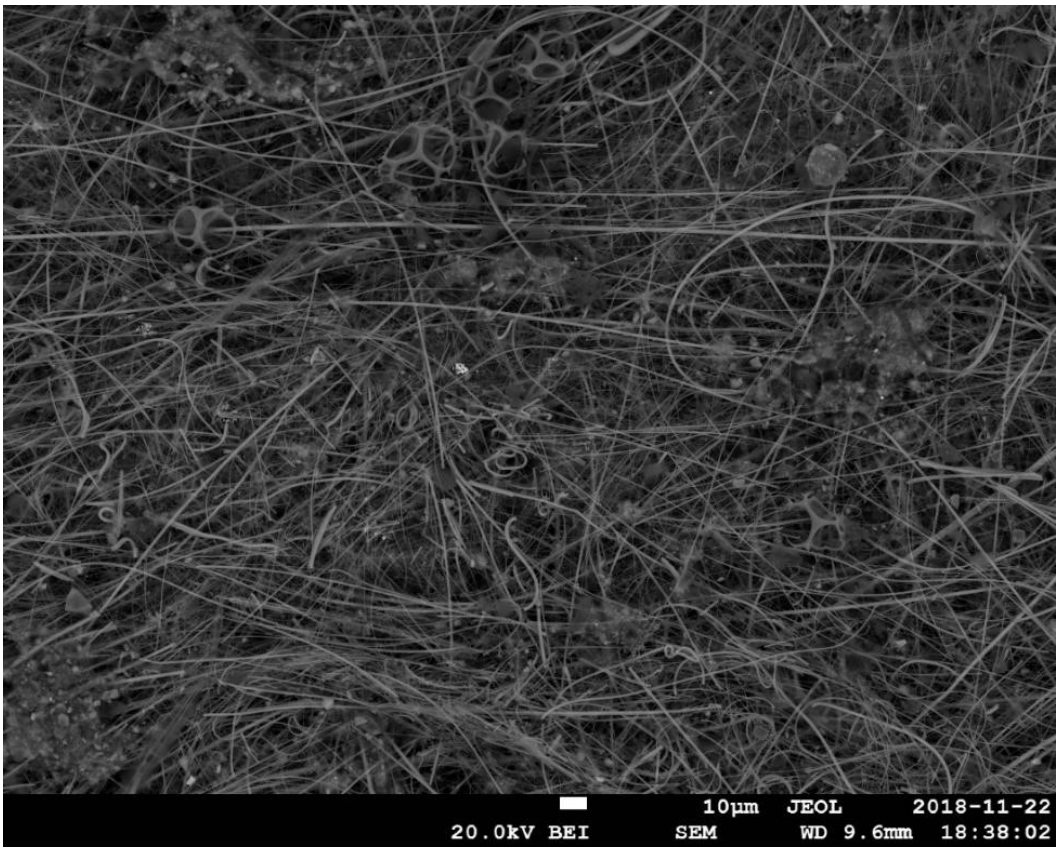

Figure B4. Fraction: Fine/Intermediate/Coarse (amounts in scale 1 – 10).

Station: D10 Fraction: 3/4/1 LISST-100X (in %): 23/40/37

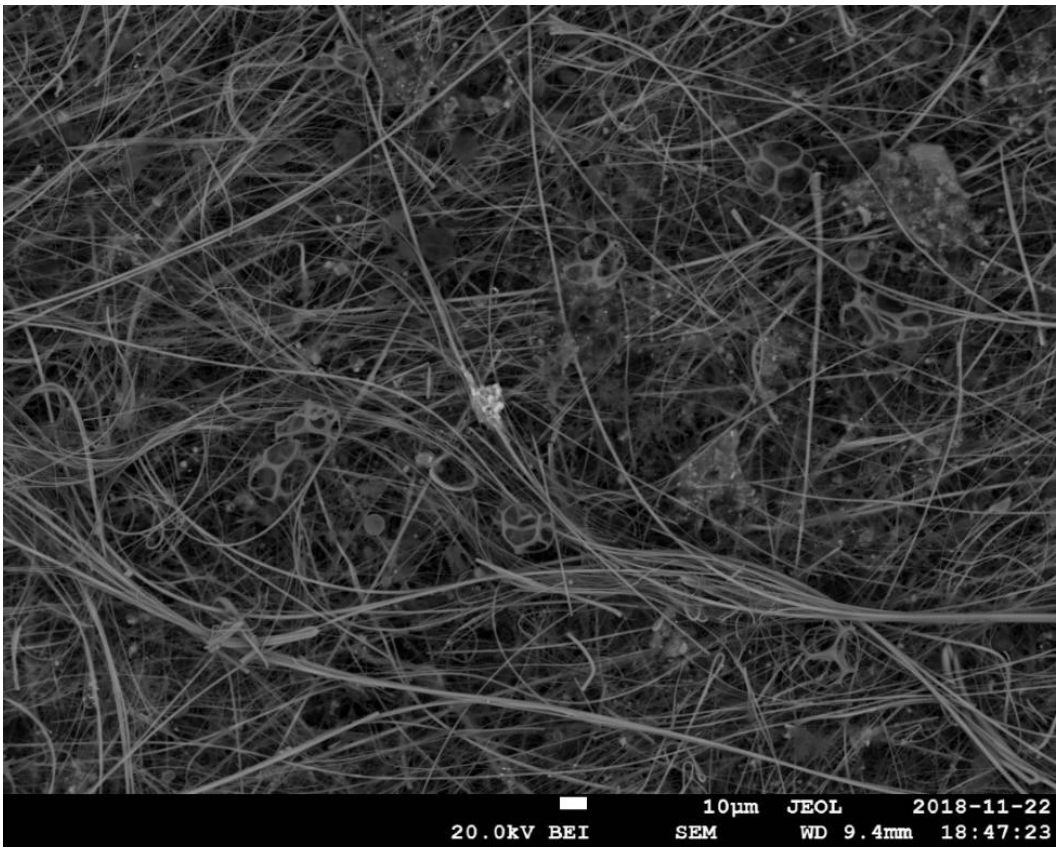

Figure B5. Fraction: Fine/Intermediate/Coarse (amounts in scale 1 – 10).

Station: D35 Fraction: 6/4/1 LISST-100X (in %): 11/17/71

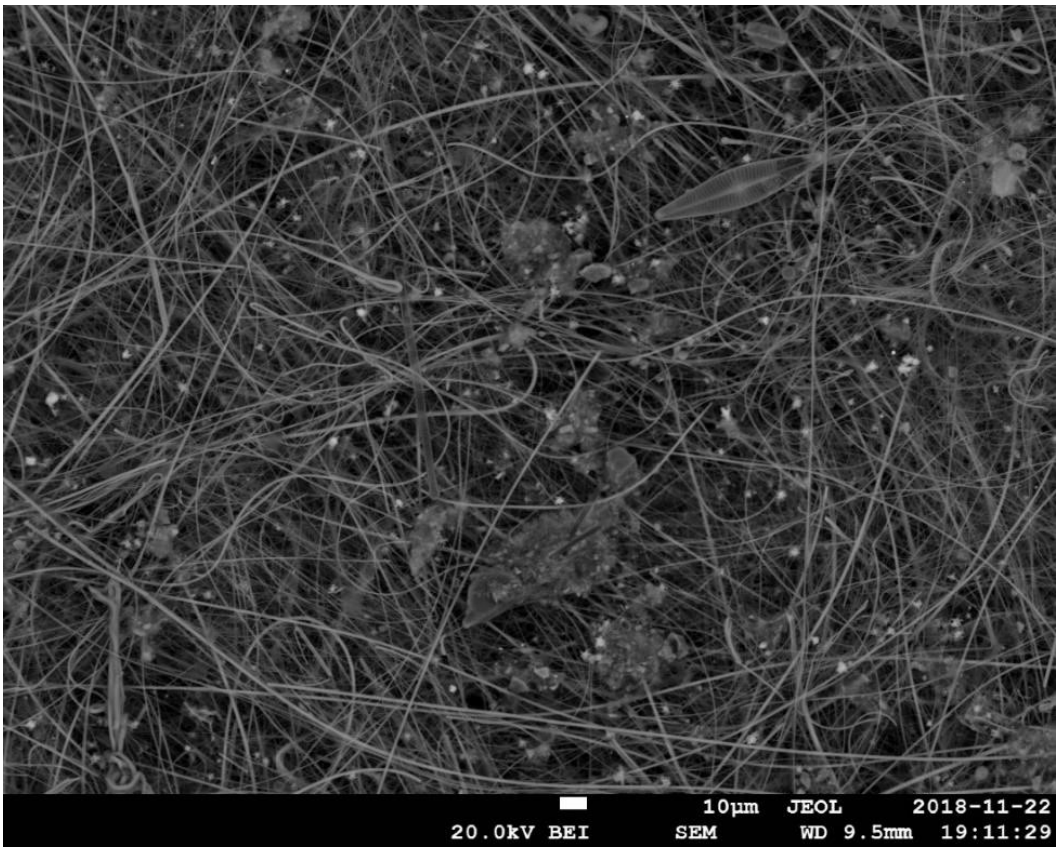

Figure B6. Fraction: Fine/Intermediate/Coarse (amounts in scale 1 – 10).

Station: E0 Fraction: 5/6/2 LISST-100X (in %): 37/38/25

Figure B7. Fraction: Fine/Intermediate/Coarse (amounts in scale 1 – 10).

Station: F0 Fraction: 5/5/3 LISST-100X (in %): 34/40/26

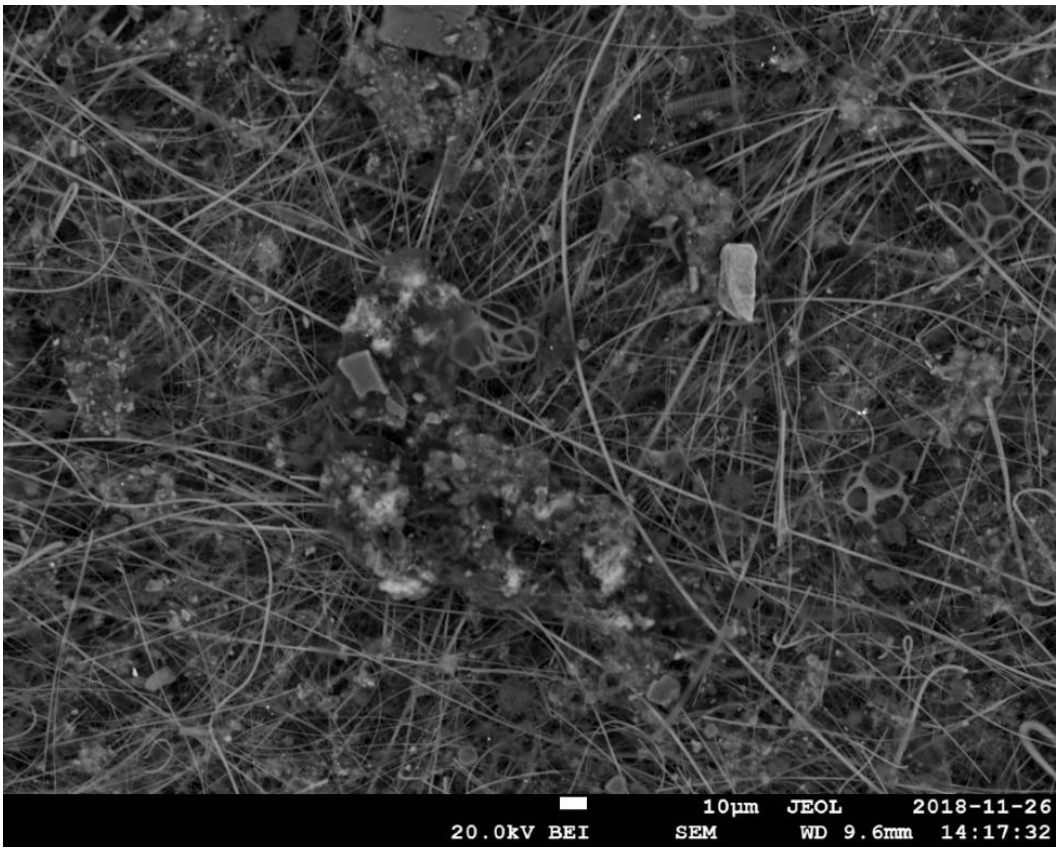

Figure B8. Fraction: Fine/Intermediate/Coarse (amounts in scale 1 – 10).

Station: G4 Fraction: 1/3/1 LISST-100X (in %): 25/30/45

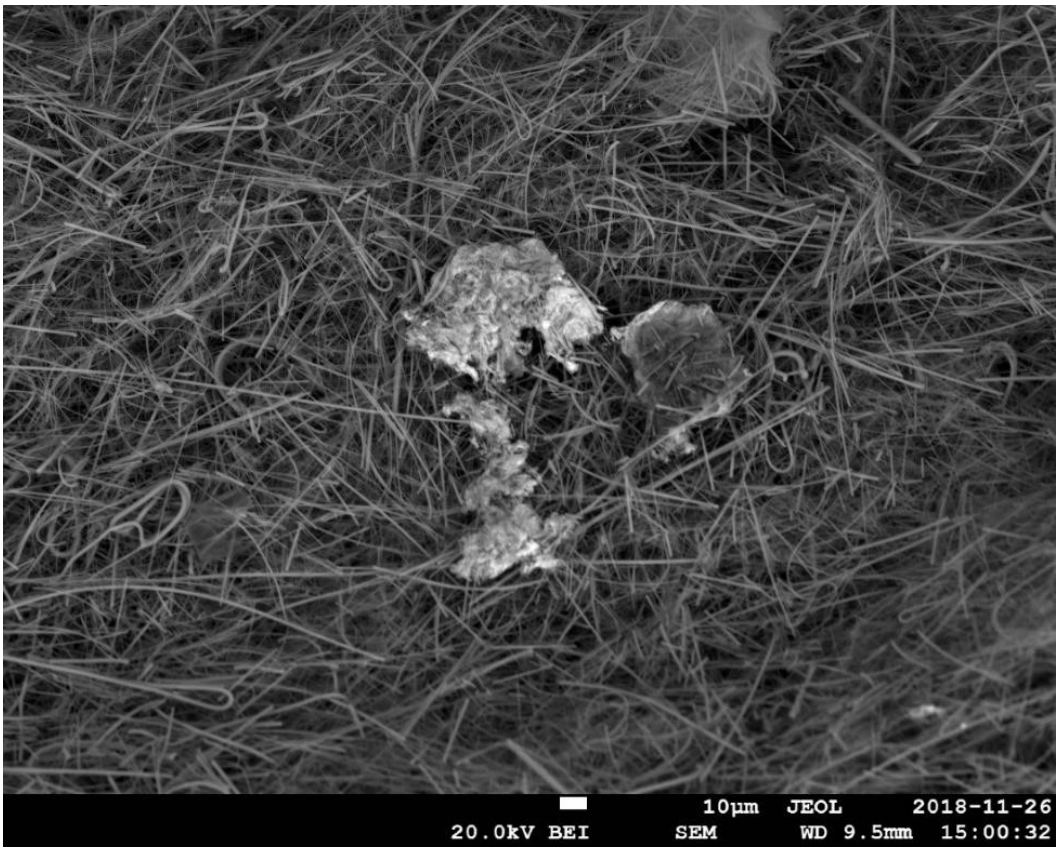

Figure B9. Fraction: Fine/Intermediate/Coarse (amounts in scale 1 – 10).

Station: H4 Fraction: 5/4/3 LISST-100X (in %): 30/38/32

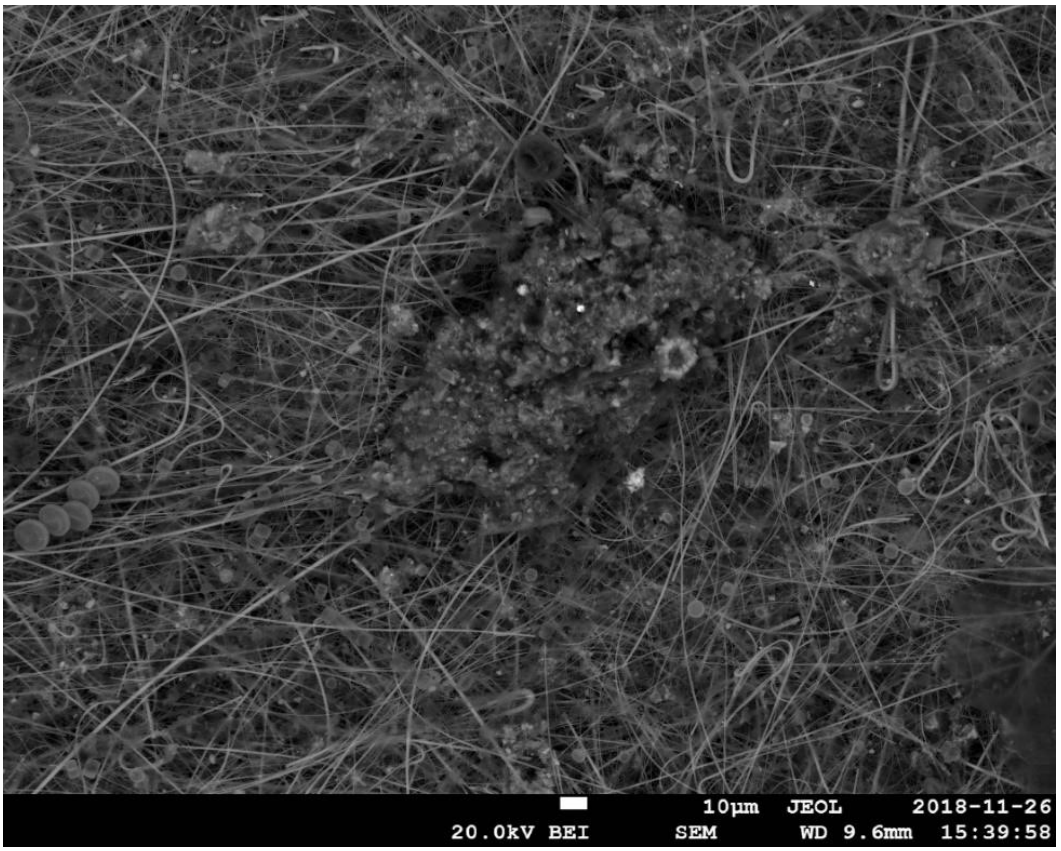

Figure B10. Fraction: Fine/Intermediate/Coarse (amounts in scale 1 – 10).

Station: J2 Fraction: 3/3/3 LISST-100X (in %): 35/49/16

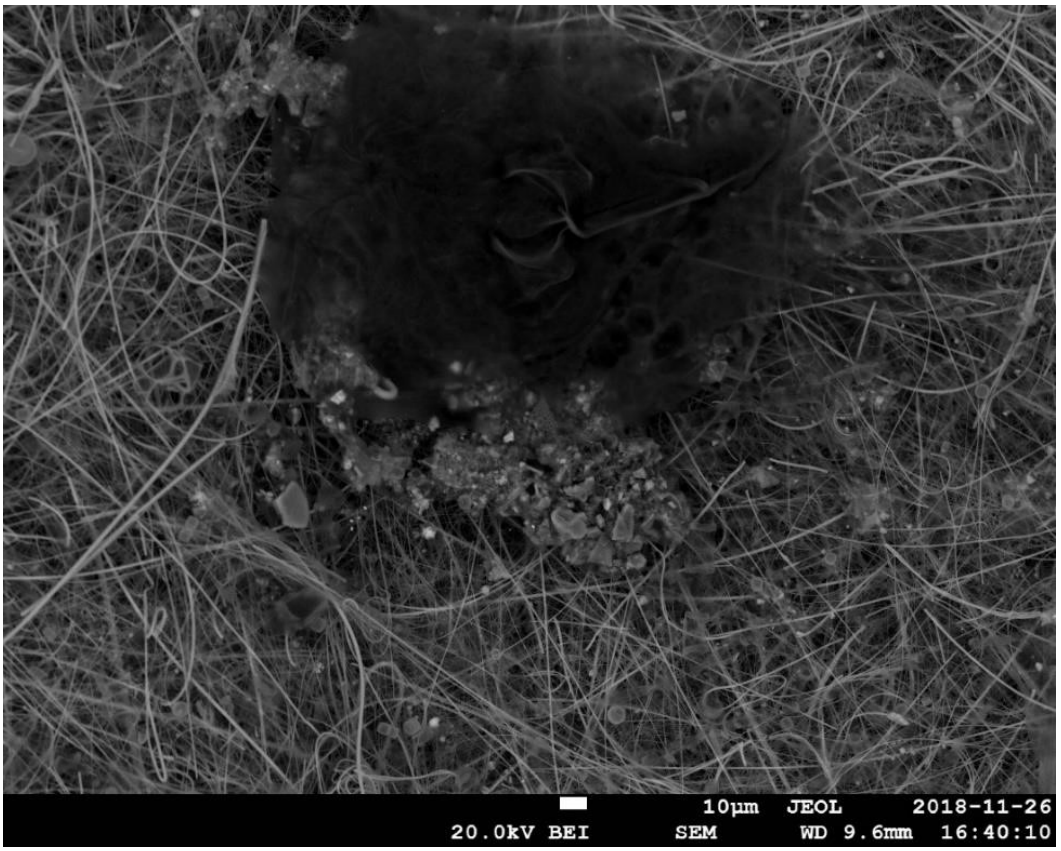

Figure B11. Fraction: Fine/Intermediate/Coarse (amounts in scale 1 – 10).

Appendix C: Manganese concentrations (total)

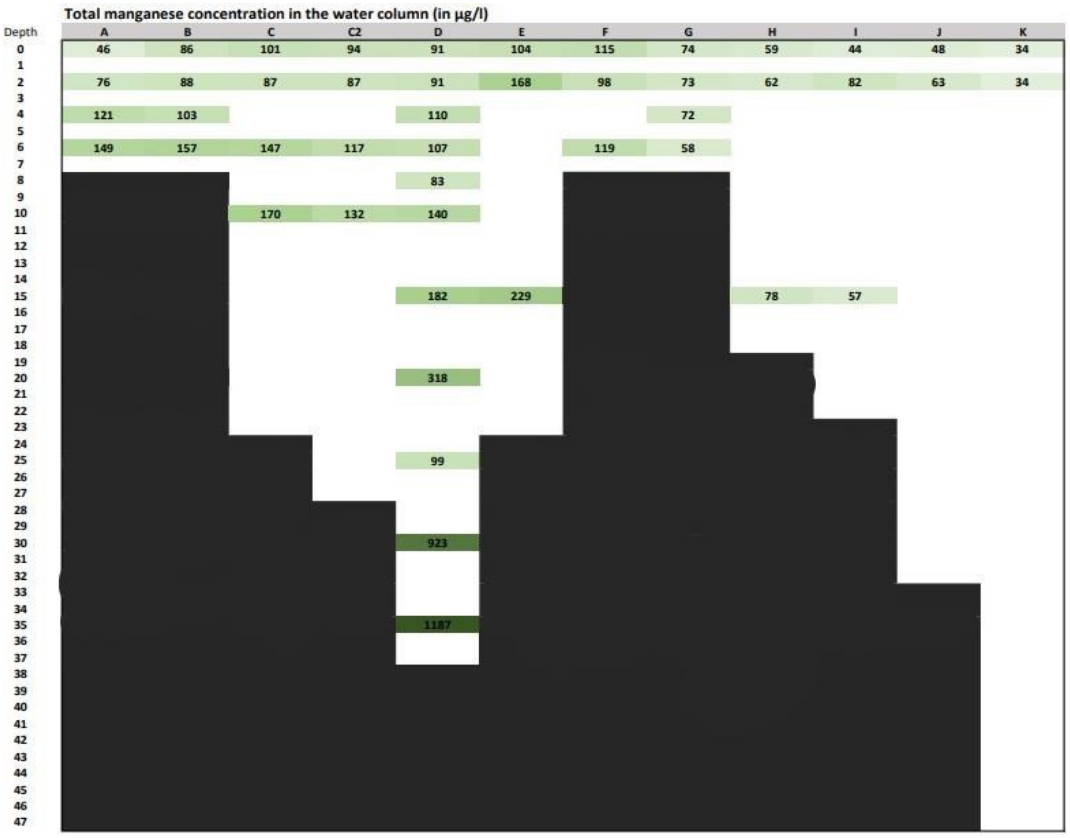

Depth	A	B	C	C2	D	E	F	G	H	I	J	K
0	46	86	101	94	91	104	115	74	59	44	48	34
1												
2	76	88	87	87	91	168	98	73	62	82	63	34
3												
4	121	103			110			72				
5												
6	149	157	147	117	107		119	58				
7												
8					83							
9												
10			170	132	140							
11												
12												
13												
14												
15					182	229			78	57		
16												
17												
18												
19												
20					318							
21												
22												
23												
24												
25					99							
26												
27												
28												
29												
30					923							
31												
32												
33												
34												
35					1187							
36												
37												
38												
39												
40												
41												
42												
43												
44												
45												
46												
47												

Figure C1. The total manganese (Mn) concentration along the *Pohjanpitäjänlahti* estuarine transect.